From INSTITUTE OF ENVIRONMENTAL MEDICINE (IMM)
Karolinska Institutet, Stockholm, Sweden

DEVELOPMENT OF NANOSCALE DELIVERY SYSTEMS FOR BREAST CANCER TREATMENT

Yuning Zhang

Karolinska Institutet

Stockholm 2015

Published by Karolinska Institutet.
Printed by E-print AB.

ISBN 978-91-7549-939-0

Karolinska Institutet

Institutet för Miljömedicin

Development of Nanoscale Delivery Systems for Breast Cancer Treatment

AKADEMISK AVHANDLING
som för avläggande av medicine doktorsexamen vid Karolinska Institutet offentligen försvaras i Farmakologens föreläsningssal, Nanna Svartz väg 2

Fredagen den 29 May, 2015, kl 09.00

av

Yuning Zhang

Huvudhandledare:
Associate Professor Andreas M. Nyström
Karolinska Institutet
Institutionen för Miljömedicin

Bihandledare:
Professor Bengt Fadeel
Karolinska Institutet
Institutionen för Miljömedicin

Professor Agneta Richter-Dahlfors
Karolinska Institutet
Institutionen för Neurovetenskap

Fakultetsopponent:
Professor Elizabeth R. Gillies
University of Western Ontario
Department of Chemistry and Chemical and Biochemical Engineering

Betygsnämnd:
Professor Edvard Smith
Karolinska Institutet
Institutionen för Laboratoriemedicin

Dr. Ana Teixeira
Karolinska Institutet
Institutionen för Medicinsk Biokemi och Biofysik

Professor Jöns Hillborn
Uppsala Universitet
Institutionen för Kemi
Enheten för Polymerkemi

Stockholm 2015

To my dear family

ABSTRACT

Nanoparticle (NP) assisted diagnosis and drug delivery for antitumor applications have been widely investigated in the past few decades. To date, some of them have been approved for clinical applications and many more of them are under clinical trials. Although some progress has been achieved, it is still necessary to explore novel materials for antitumor applications. The work summarized in this thesis focused on organic NPs, and evaluated engineered polymer NPs and protein-lipid NPs as antitumor drug delivery systems *in vitro*. And a multifunctional fluorinated NP system was also assessed as theranostic (the combination of therapy and diagnosis) platform.

In paper I, two types of 2,2 bis(hydroxymethyl) propionic acid (bis-MPA) based dendritic-linear (DL) polymers were synthesized. One type has the hyperbranched (HB) dendritic structure while the other has dendrons (perfectly branched structures). HBDL and DL materials were compared as drug delivery systems in respect to their synthesis difficulty, quality of micelle formation and efficiency in drug delivery. It was found that HBDL can be synthesized in large scales and drug loaded HBDL tended to have stronger efficacy compared to DL, therefore it is a promising alterative to DL in anticancer drug delivery. Further, in **paper II**, a detailed study regarding the uptake profile of a bis-MPA based hyperbranched copolymer micelle was conducted. The NP consisted of a Boltorn-H30 core (hyperbranched polyester) and PEG_{10k} hydrophilic tails. It was found that the hyperbranched NP can be internalized into breast cancer cells via clathrin-dependent and macropinocytosis-mediated pathway through a time, concentration and energy dependent process. **In paper III**, fluorinated copolymers micelles were synthesized and evaluated as theranostic system, which has both diagnostic and therapeutic functions. The consequent micelles were able to load and release doxorubicin (DOX) and demonstrated similar efficacy compared to free (non-formulated) DOX. Also these NPs could generate a detectable signal for ^{19}F-MRI *in vitro*. In **paper IV**, unimolecular NPs were developed from polyester based hyperbranched dendritic-linear polymers (HBDLPs). Such micelles were homogenous and did not have critical micelle concentration (CMC). And they were able to load DOX and delivery the drug into breast cancer cells. One HBDLP based NP containing a fluorinated polymer fragment was also synthesized to prove that these unimolecular systems are potentially useful as theranostic platforms. In **paper V**, histamine functionalized copolymer micelles were developed in order to introduce pH responsive property to NPs and achieve endo-lysosomal escape. These NPs were non-toxic and capable of loading and release DOX. Drug loaded NPs exhibited significant enhanced inhibition of mitochondria function in breast cancer cells during short periods (12 h) compared to free DOX. Although the expected pH responsive behaviour was not observed for the *in vitro* drug release model, NPs with histamine functionalization demonstrated partly endo-lysosomal escape property, in particular for those with 50% histamine modification. Intracellular tracking of NPs revealed that they could escape from endo-lysosomes and relocate DOX into mitochondria and the nuclei. In **paper VI**, lipoprotein like NP systems were developed by incorporating Saposin A, phospholipids and selected

hydrophobic cargos. Such systems were shown to have promise as drug delivery platforms and to serve as NP based vaccine stabilizers.

LIST OF SCIENTIFIC PAPERS

This thesis is based on the following papers:

I. Yvonne Hed*, **Yuning Zhang***, Oliver C.J. Andren, Xianghui Zeng, Andreas M. Nyström, Michael Malkoch. Side-by-side comparison of dendritic-linear hybrids and their hyperbranched analogs as micellar carries of chemotherapeutics. *Journal of Polymer Science part A: Polymer Chemistry*, 2013, 51, 3992-3996.
*contributed equally

II. Xianghui Zeng, **Yuning Zhang**, Andreas M. Nyström. Endocytic uptake and intracellular trafficking of bis-MPA-based hyperbranched copolymer micelles in breast cancer cells. *Biomacromolecules*, 2012, 13, 3814-3822.

III. Christian Porsch*, **Yuning Zhang***, Åsa Östlund, Peter Damberg, Cosimo Ducani, Eva Malmström, Andreas M. Nyström. *In vitro* evaluation of non-protein adsorbing breast cancer theranostics based on ^{19}F-polymer containing nanoparticles. *Particle & Particle Systems Characterization*, 2013, 30, 381-390.
*contributed equally

IV. Christian Porsch, **Yuning Zhang**, Cosimo Ducani, Francisco Vilaplana, Lars Nordstierna, Andreas M. Nyström, Eva Malmström. Toward unimolecular micelles with tunable dimensions using hyperbranced dendritic-linear polymers. *Biomacromolecules*, 2014, 15, 2235-2245.

V. **Yuning Zhang**, Pontus Lundberg, Maren Diether, Christian Porsch, Caroline Janson, Nathaniel A. Lynd, Cosimo Ducani, Michael Malkoch, Eva Malström, Craig J. Hawker, Andreas M. Nyström. Histamine-functionalized copolymer micelles as a drug delivery system in 2D and 3D models of breast cancer. *Journal of Materials Chemistry B*, 2015, 3, 2472-2486.

VI. Jens Frauenfeld, Robin Löving, **Yuning Zhang**, Lin Zhu, Caroline Jegerschöld, Fatma Guettou, Per Moberg, Christian Löw, Andreas M. Nyström, Henrik Garoff, Pär Nordlund. A multi-functional nanoparticle system based on a small human protein.
Submitted manuscript 2014

Additional relevant papers not included in the thesis:

I. Xianghui Zeng, **Yuning Zhang**, Zhihua Wu, Pontus Lundberg, Michael Malkoch, Andreas M. Nyström. Hyperbranched copolymers micelles as delivery vehicles of doxorubicin in breast cancer cells. *Journal of Polymer Science part A: Polymer Chemistry***,** 2012, 50, 280-288.

II. Zhihua Wu, Xianghui Zeng, **Yuning Zhang**, Neus Feliu, Pontus Lundberg, Bengt Fadeel, Michael Malkoch, Andreas M. Nyström. Linear dendritic polymeric amphiphiles as carriers of doxorubicin – *in vitro* evaluation of biocompatibility and drug delivery. *Journal of Polymer Science part A: Polymer Chemistry*, 2012, 50, 217-226.

III. Pontus Lundberg, Nathaniel A. Lynd, **Yuning Zhang,** Xianghui Zeng, Daniel V. Krogstad, Tim Paffen, Michael Malkoch, Andreas M. Nyström, Craig J. Hawker. pH-triggered self-assembly of biocompatible histamine-functionalized triblock copolymers, *Soft Matter*, 2013, 9, 82-89.

IV. Neus Feliu, Pekka Kohonen, Jie Ji, **Yuning Zhang**, Hanna L. Karlsson, Lena Palmberg, Andreas M. Nyström, Bengt Fadeel, Next Generation Sequencing Reveals Low-Dose Effects of Cationic Dendrimers in Primary Human Bronchial Epithelial Cells, *ACS Nano*, 2015, 9, 146-163.

CONTENTS

LIST OF ABBREVIATIONS

ATP	Adenosine triphosphate
ATCC	American Type Culture Collection
ATRP	Atom transfer radical polymerization
BBB	Blood brain barrier
BBEMA	2-(2- bromoisobutyryloxy)ethyl methacrylate
Bis-MPA	2,2 bis(hydroxymethl) propionic acid
BN-PAGE	Blue native polyacrylamide gel electrophoresis
C	Complement
CARPA	Complement activation-related pseudoallergy
CMC	Critical micelle concentration
CuAAC	Copper(I)-catalyzed azide–alkyne cycloaddition
CT	Computed tomography
DDS	Drug delivery system
DL	Dendritic linear
DLS	Dynamic light scattering
DNA	Deoxyribonucleic acid
DOX	Doxorubicin
DOX-NP	Doxorubicin loaded nanoparticle
DMEM	Dulbecco's modified Eagle medium
DMF	Dimethylformamide
EPR	Enhanced permeability and retention
FACS	Fluorescence-activated cell sorting
FBS	Fetal bovine serum
FDA	Food and Drug Administration
FITC	Fluorescein isothiocyanate
HBDL	Hyperbranched DL hybrids
HBDLP	Hyperbranched dendritic-linear polymers
HA	Hexyl acrylate
IONPs	Iron oxide nanoparticles
MAA	Methacrylic acid

MALDI-TOF	Matrix assisted desorption ionization time of flight
MRI	Magnetic resonance imaging
mRNA	Messgener RNA
MTT	3-(4,5-dimethylthiazol-2-yl)-2,5-diphenyltetrazolium bromide
MW	Molecular weight
MWCO	Molecular weight cut-off
NBD	7-nitro-2-1,3-benzoxadiazol-4-yl
NMR	Nuclear magnetic resonance
NPs	Nanoparticles
OEGMA	Oligo(ethylene glycol) methyl ether methacrylate
P	Poly
PAGE	Poly(allyl glycidyl ether)
PAMMA	Polyamidoamine
pDNA	Plasma DNA
PEG	Polyethylene glycol
PEO	Poly(ethylene oxide)
PET	Positron emission tomography
PI	Propidium iodide
RES	Reticuloendothelial system
RGD	Arginine-glycine-aspartic
rHDL	High-density lipoprotein
Salipro-NP	Saposin-lipoprotein nanoparticle
scFV	Single-chain antibody fragment
SCV(C)P	Self-condensing vinyl (*co*) polymerization
SEC	Size-exclusion chromatography
SEC-MALLS	Size exclusion chomatography - multi-angle laser light scattering
SDS	Sodium dodecyl sulfate
SDS-PAGE	Sodium dodecyl sulfate polyacrylamide gel electrophoresis
siRNA	Small interfering RNA
SPECT	Single photon emission computed tomography

SPION	Superparamagnetic iron oxide nanoparticle
TBBPE	1,1,1-tris(4-(2-bromoisobutyryloxy)phenyl)-ethane
TEM	Transmission electron microscopy
Tf	Transferrin
TFEMA	Trifluoroethyl methacrylate
TfR	Transferrin receptor
UV-*vis*	Ultraviolet-visible spectroscopy

1 INTRODUCTION

1.1 BREAST CANCER AND THE MODULAR DRUG

Breast cancer is one of the most prevalent malignant diseases in women in Western countries. Although the death rate of breast cancer from the primary tumor is not the highest compared to other type of carcinomas, its metastases often lead to other deadly cancers.[1] As a result, early detection and treatment of breast cancer is imperative and worthy of study. Driven by this goal, nanotechnology has played an irreplaceable role in establishing novel diagnostic and therapeutic approaches. In 2005, Abraxane (albumin-entrapped paclitaxel) was approved by the Food and Drug Administration (FDA) as the first nanomedicine for metastatic breast cancer treatment, and this drug has demonstrated improved efficacy compared to pure paclitaxel.[2,3] In addition, nanoparticle (NP)-assisted imaging and detection of breast cancer has also been reported.[4,5] For instance, iron oxide NPs (IONPs) conjugated with recombinant amino-terminal fragment of urokinase-type plasminogen activator could act as a contrast agent of magnetic resonance imaging (MRI) for breast cancer diagnosis *in vivo*.[6]

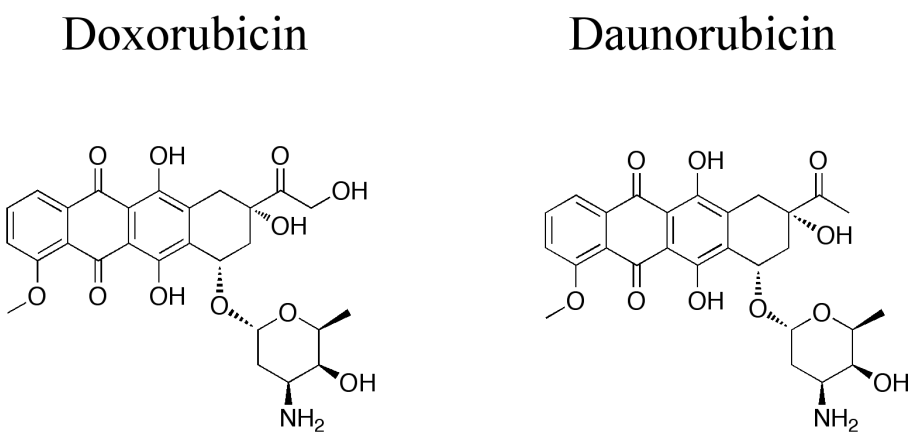

Figure 1. Chemical structures of doxorubicin and daunorubicin.

Anthracycline antitumor drugs, including both doxorubicin (DOX) and daunorubicin (Figure 1), can intercalate into the DNA of rapidly growing cells like cancer cells and can inhibit their proliferation.[7] However, the administration of anthracylines can induce severe cardiotoxicity among other side-effects,[8] and this limits their clinical usefulness. Unlike other common chemotherapeutics such as paclitaxel and gemcitabine, the intrinsic fluorescent properties of the anthracyclines make them suitable modular drugs in nanoparticle-assisted drug delivery research. In fact, early in 1995 a polyethylene glycol (PEG)-coated (PEGylated) liposomal DOX (Doxil) was approved by the FDA for treatment of Kaposi's sarcoma, and the indications were later expanded to include ovarian cancer and multiple myeloma therapy.[9] Doxil demonstrated better efficacy and reduced cardiotoxicity compared to free DOX,[10] and since then many different nanocarriers with encapsulated DOX have been designed and

evaluated as therapeutics against breast cancer.[11-13] In this thesis, we employed DOX and daunorubicin as model drugs to assess polymer-based and protein-lipid based NPs as drug delivery systems (DDSs).

1.2 NANOMEDICINE IN GENERAL

1.2.1 A brief history

Nanomedicine has been one of the most rapidly growing research areas in the past two decades. The term describes a large group of nanoscale devices, usually with dimensions ranging from 1 nm to 1000 nm,[3] that are employed in biomedical applications, including biosensing,[14-16] tissue engineering,[17-19] bioimaging,[20-22] diagnosis,[23-26] and therapy[27-29] for a range of diseases.

Table 1. Examples of nanoparticles in clinical studies

Name	Comments	Indication	Phase	Ref
BIND-014	Docetaxel, Polylactide (PLA) and PEG. targeting, controlled release	Solid tumors	II	[30]
CALAA-01	siRNA, cyclodextrin, PEG. targeting	Solid tumors	I	[31]
CPX-1	Irinotecan HCl/floxuridine, liposome.	Acute myeloid leukemia	II/III	[32]
SEL-068	Nicotine, PLAG, lipid, PEG. Synthetic vaccine particle (tSVP)	Smoking cessation	I	[33]
SP1049C	Doxorubicin, Pluronic polymeric micelle.	Advanced adenocarcinoma	II/III	[34]
Nanotax	Paclitaxel, polymeric nanoparticle	Peritoneal neoplasms	I	[35]
2B3-101	Doxorubicin, liposome, Glutathione targeting	Brain metastases of breast cancer	I/II	[36]

The dawn of nanomedicine started in the 1950s and 1960s when two nano-systems, polymer-drug conjugates (with a single polymer chain) and liposomes, were invented by Jatzkewitz and Bangham, respectively.[10]After that, albumin-based and polymer-based NPs were developed in 1970s.[37] Another remarkable breakthrough was achieved in the 1980s by Maeda *et al.*[38] who discovered the enhanced permeability and retention (EPR) effect,[39] which forms the cornerstone of passive targeting of solid tumors and has initiated the rapid growth of NP-assisted cancer therapy systems. Since then, NPs have been extensively investigated for use as DDSs, and methods for controlled release,[40-44] PEGylated systems,[45,46] targeted delivery,[29,47,48] and gene delivery[49-53] have all been developed. To date, dozens of nanomedicines have passed clinical trials and been approved by the FDA for clinical use, and many more of them are currently in clinical trials (Table 1) or under investigation in the lab. These nanomedicines are designed to target various medical problems such as infection,[54] diabetes,[55] cancer,[56] and other diseases.[33,57,58]

1.2.2 Classifications of nanomedicine

The term 'nanomedicine' can be defined as the use of nanotechnology to solve biomedical problems. [10] There is currently no unified classification of nanomedicines because of the broad range of members in this diverse family. However, most nanomedicines can be classified as NPs as long as they have a particle-like morphology and nanoscale dimensions. Sometimes the term 'nanovector' is used for molecule delivery agents or in bioimaging applications to describe the hollow or solid NPs that serve to transport other molecules.[3] Based on their chemical composition, NPs can be classified as summarized in Table 2.

Table 2. Classification of NPs based on their compositions.				
NPs	Inorganic NP	Metal NP	Gold (colloid), silver, metal oxides, *etc.*	
			Superparamagnetic iron oxide nanoparticle (SPION)	supra para magnetic
		Non-metal NP	Silica NP	Mesoporous
			Carbon nanotube	Cylinder
	Organic	Bio-derived NP	Liposome	
			Polyamino acid NP	Natural polymer NP
			Polypeptide NP	
			DNA NP	
			Polysaccharide NP	
		Engineered Polymer NP	Polymer-drug conjugates	
			Micelles (copolymer)	Linear, star like, hyperbranched
			Dendrimers and Dendrons	Unimolecular
		Organic hybrids	Conjugated or encapsulated with polymer	
	Hybrids		Most inorganic NPs need lipid or polymer coating or modifications	

1.2.3 Structure and advantages of nanomedicine

Figure 2 shows the typical structure of a NP for drug delivery and diagnostic applications. Such NPs usually consist of three parts: a core structure, therapeutic cargo or contrast agent (or both for theranostic NPs), and a hydrophilic surface with suitable modifications that provide good solubility, enhanced blood circulation time, and improved targeting properties.[3] Amphiphilic polymer micelles can encapsulate insoluble drugs such as paclitaxel in the hydrophobic core and thus enhance the drugs' solubility.[59,60] Due to their reduced protein absorption, NPs with PEG protection demonstrate enhanced blood

circulation time by evading reticuloendothelial system (RES).[61-64] Moreover, the shielding of NPs with PEG is helpful in reducing the side effects and enhancing the efficacy of chemotherapeutics.[23,65,66] For instance, Doxil (a liposome-based nanomedicine with a payload of DOX) treated women with metastatic breast cancer has demonstrated similar overall survival rate but reduced cardiotoxicity (by evaluating left ventricular ejection fraction and congestive heart failure) compared to free DOX [67] Another study also showed that patients receiving Doxil had lower level of clinical cardiotoxicity of compared to DOX in cumulative doses of 500 mg per m^2 (equivalent DOX dose).[68] Besides, the core-shell structure of a NP can also help protect its payload, and this is particularly useful in NP-assisted gene therapy, which requires the proper delivery of plasma DNA (pDNA), messenger RNA(mRNA), or small interfering RNA(siRNA) to the target while shielding the DNA/RNA from degradation by enzymes in the blood stream.[69-71] In addition, bio-functional moieties can be introduced onto the surface of NPs improving the biodistribution of NPs at the tumor area due to the active targeting effect.[72-74] One example is CALAA-01, currently in phase I clinical trials, which utilizes transferrin as the targeting molecules to improve the siRNA delivery to solid tumors on which transferrin receptors are overexpressed.[31]

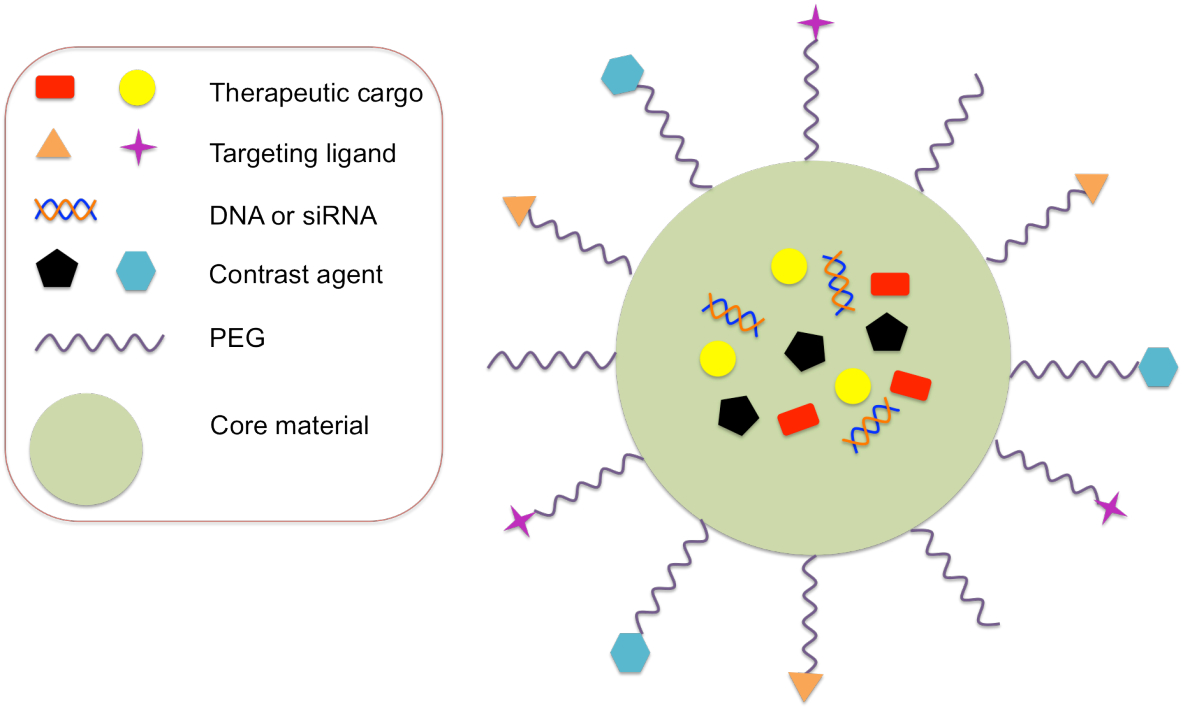

Figure 2. The structure of a typical nanomedicine.

The fundamental advantage of nanomedicines compared to conventional medicines is that they can be designed with multifunctionality in mind.[75,76] As mentioned above, the core area of the NPs can be used to carry therapeutic payloads. In addition, nanomedicines can be designed to carry imaging payloads such as Gd^{3+},[77] SPIONs,[78] radionuclides,[79] radio opaque iodine,[80] or Tc-99m,[81] and can be traced with modern diagnostic devices like magnetic resonance imaging (MRI), positron emission tomography (PET), computed tomography (CT), and single photon emission computed tomography (SPECT).[82] In

particular, polymer-based NPs can be used for diagnostic purposes by simply conjugating fluorine-containing copolymers to the system, which makes them detectable by ^{19}F-MRI.[83] This approach is considered promising for solid tumor detection based on three aspects: 1)^{19}F is the only nature isotope of fluorine and it can only be found in teeth and bones in human body, and leading to minimal background influence.[84] 2) Fluorinated polymer can have a high degree of equivalent F to generate strong signal even though F has 17% weaker signal than proton.[84] 3) Fluorinated polymers can be covalently linked to other polymers to form copolymer micelles, there is no need to encapsulate or install other contrast agents in the NPs to achieve MRI imaging.

In addition, the large surface area to volume ratio of NPs allows various types of functional moieties to be attached and to confer special functions.[85] For example, NPs that contain cyclic arginine-glycine-aspartic (RGD) peptides can specifically target integrin $\alpha_v\beta_3$ overexpression on endothelial tumor cells.[86-88] Moreover, functional moieties can allow the NP to penetrate through some biological barriers. For example, it has been reported that TAT (YGRKKRRQRRR) peptides will help NPs to pass through the blood brain barrier (BBB) thus allowing delivery of drugs to the brain to treat infections.[89]

1.3 NANOMEDICINES *VS.* TUMORS

One of the most common areas of nanomedicine application is in the field of oncology, and these agents are used for both tumor diagnosis and therapy. The main rationale for using NPs in biomedical application is that they can be designed to have several desired functions. Several basic requirements have been proposed to define a successful nanomedicine, including high efficacy per dose for both imaging and therapeutic applications, targeting to the tumor area, and avoiding degradation before arriving at its target.[3]

1.3.1 Issues regarding anticancer NP development

Several issues influence the design of a successful NP. The first thing to consider is the strategy of the NP's administration, which normally dictates certain requirements in its design. In general, a nanomedicine can be administered into the human body via inhalation, oral administration, or injection.[90-92] The inhalation strategy is limited to the delivery of nanomedicines to the lungs due to problems with aggregation.[93] Orally administrated NPs have been reported for insulin delivery,[94] and this requires NPs to have strong pH stability to survive the acidic environment and avoid enzymatic degradation in the gastrointestinal tract.[95] Currently, the majority of nanomedicines for cancer treatment are administrated by intravenous injection.[96] This requires the NPs to have a long blood circulation time and low to no immunoreactivity. To this end, the size and surface properties for biological interactions are also crucial parameters to consider.[10]

Size is important regarding the circulation time of NPs in the blood stream; if they are too small or too large this might cause unwanted clearance before the NPs reach their target. There are evidences that NPs smaller than 5 nm can be easily filtered out from bloodstream via the kidney[10,97] and transported to the bladder within 15 min of administration.[98] NPs that are too large can be removed by sinusoids and clearance via RES.[99] Considering the requirement for NPs to accumulate at the tumor site via the EPR effect, the ideal size of NPs ranges from 10–500 nm.[99]

In order to avoid rapid clearance, surface modification of NPs is necessary. The most common strategy to evade immunological interactions is to decorate the NP with PEG chains.[64,100,101] PEG has been shown to be inert to bio-recognition due to reduced protein absorption in biophysical environments, and this leads to reduced immunological response, reduced RES clearance, and prolonged blood circulation time.[100,102,103] However, the presence of PEG on surface of liposomes surface have been reported to promote complement (C) activation, which results in C activation-related pseudoallergy (CARPA) that is considered as the major cause of hypersensitivity reactions.[104] All of the three pathways for C activation, the classical pathway, alternative pathway and lectin pathway have been found to contribute to PEG promoted C activation due to the presence of anti-PEG antibodies, ‘‘protein partitioning and exclusion’’ and ficolin/MASP-2-mediation, respectively.[105-107] Moreover, the concentration of PEG on surface or the linker to NP may influence the C activation.[108,109] This presents a paradox: PEG enhances nanomedicine’s efficacy but can also promote C activation in some patients. A possible explanation for this was proposed by Moghimi and Szebeni, who pointed out that PEG helps the coated particles to evade macrophages uptake regardless of C activation.[104,110,111]

1.3.2 Targeting solid tumors

The discovery of EPR effects by Maeda and colleagues in the 1970s is considered to be the foundation of nanomedicine research for solid tumor therapy (Figure 3).[38,39] This effect refers to the phenomenon in which NPs (50–200 nm) can selectively accumulate at a tumor site compared to small-molecule drugs. The EPR effect is caused by both the leaky vasculature and slow lymphatic drainage of large particles at the tumor site, and it constitutes a passive targeting mechanism for solid tumors.[112-114] Thus significant efforts have been put into designing NPs that can target solid tumors based on the EPR effect. The overall strategy is to enhance the blood circulation time of NPs to allow them to reach the tumor area and to accumulate there. In particular, NPs coated with inert molecules such as PEG reduce protein opsonization and phagocytic elimination.[96]

Besides passive targeting, active targeting strategies have also been investigated. A common strategy is to attach molecules to the surface of the NP that have higher affinity for receptors on tumor cells so as to enhance receptor-mediated uptake. Small molecules like folic acid[115] and transferrin,[116] aptamers,[48] peptides,[89] and antibodies[117] have been widely

explored for active targeting of NPs. One successful example currently in clinical trials is BIND-014, which is a polymer-based NP for targeted delivery of docetaxel to prostate-specific membrane antigen-bearing solid tumors.[30] Another one in clinical trial is a lipid base nanomedicine, SGT-53, which carries a pDNA encoding wild type p53 tumor suppressor and has a single-chain antibody fragment (scFV) that targets transferrin receptor (TfR) on tumor cells.[118-120] Other nanomedicines with Tf conjugation, such as MBP-426 and CALAA-01, are also under clinical trials for cancer treatment via targeting TfR on tumor cells. [31,118,121]

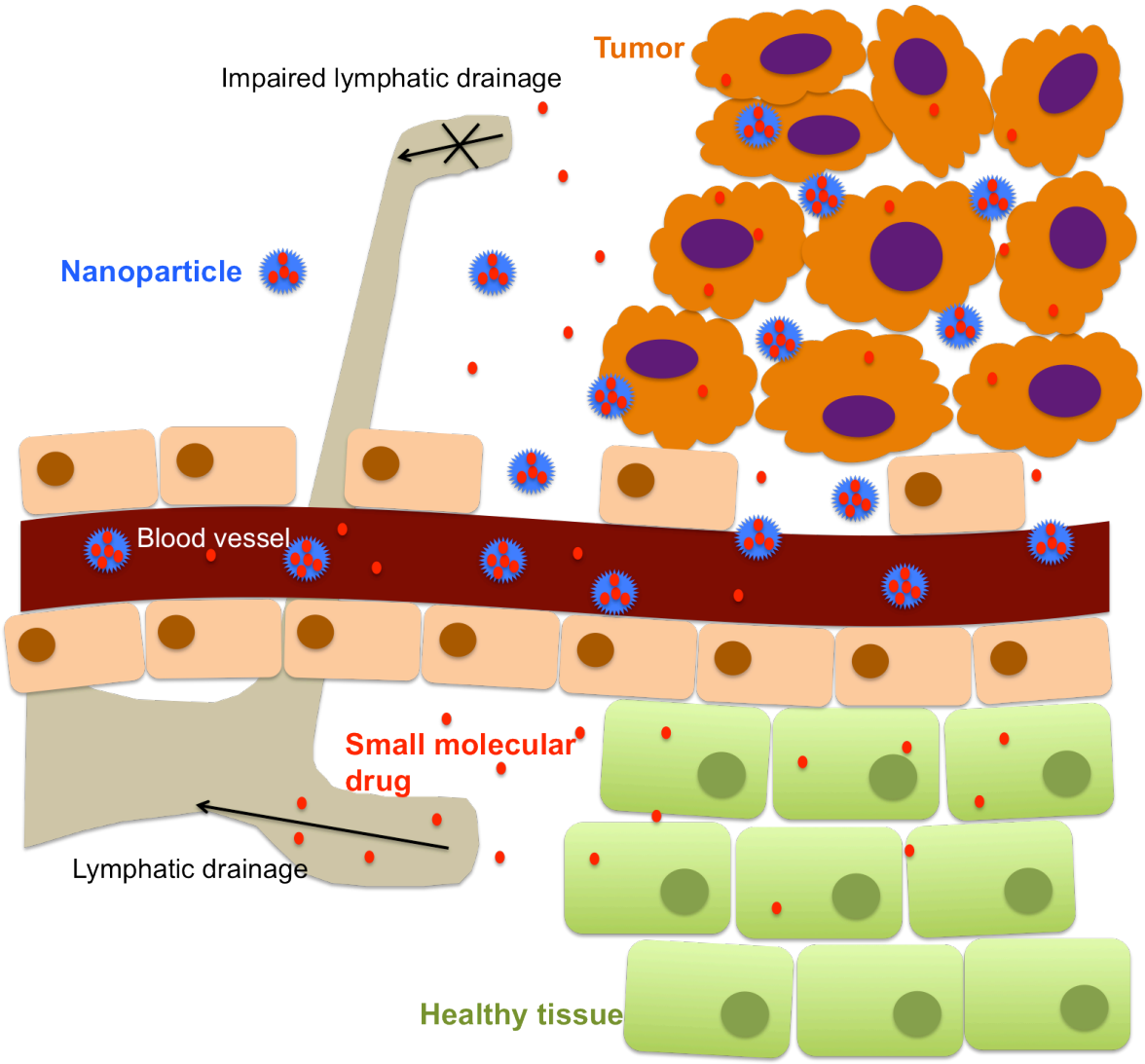

Figure 3. Illustration of the EPR effect. NPs can penetrate to tumor tissue through the leaky vasculature and be trapped there due to the slow lymphatic drainage of large particles at the tumor site.

The benefits of active targeting are still debated. Dawson *et al.* reported that transferrin-labeled NPs can lose their targeting capability in protein-rich environments, due to the

formation of a protein corona.[122] Park *et al.* demonstrated through *in vivo* experiments that antibody directed NPs did not increase tumor localization via active targeting but enhanced cancer cell uptake.[123] Similar effects was also observed by *Davis et al.* showing that Tf-targeted NPs had similar biodistribution and tumor localization but more effective siRNA delivery compared to non-targeted NPs, suggesting the Tf ligand enhanced internalization rather than localization of NPs in tumor cells.[124] Moreover, even if a targeting moiety is successfully linked to an NP and remains functional, there is still no guarantee that the receptor is only over-expressed on the target cell population.[96] This is another drawback to the use of folic acid or transferrin-labeled NPs to specifically target tumor cells because receptors for these molecules are expressed on several types of cells.[125,126] Based on these concerns, the efforts of this thesis were only focused on exploring NPs that can achieve passive targeting.

1.3.3 Diagnostic function

The use of conventional diagnostic agents such as chelated Gd^{3+} for MRI and radionucleotides for SPECT and PET are hindered by their short lifetime in the blood circulation and their poor biodistribution at the tumor site.[113] The development of nanomaterials has provided a new way to formulate contrast agents for the diagnosis of tumors. Some types of NPs can act as contrast agents by themselves due to their intrinsic properties. For instance, metal-based NPs like SPIONs can serve as imaging agents for MRI due the their intrinsic magnetic resonance property.[127] Gold NPs can generate good contrast in human tissues making them promising for CT applications.[128]

In most cases, however, NPs with diagnostic function are formulated by integrating contrast agents within the nanomaterials. Incorporated with suitable imaging modalities, NPs can serve as contrast agents in modern medical imaging techniques including CT, MRI, PET, SPECT, and ultrasound.[129] Inorganic NPs like mesoporous silica NPs can be designed to carry different types of imaging modalities for different diagnostic strategies.[130] To date, organic NPs including both bio-derived (peptides and lipids) and engineered polymers have been widely used as carriers of both imaging agents and therapeutic molecules due to their good biocompatibility. Polymer modification is very common in the development of inorganic NPs for imaging applications. Such modification imparts the system with better solubility, better biocompatibility, and longer blood circulation time. The most common strategy is adding a hydrophilic polymer such as PEG to the inorganic NPs. Recently, pure polymer NPs by themselves have been shown to be useful as contrast agents for MRI imaging. Morel *et al.* applied perfluoropolyether to label dendritic cells and achieved *in vivo* tracking of those cells in mice using ^{19}F-MRI.[131] Later Wooley *et al* developed trifluoroethyl methacrylate (TFEMA) contained amphiphilic polymer micelles that can generate detectable ^{19}F-MRI signal and deliver DOX for cancer treatment.[132,133]

1.3.4 Anticancer drug delivery

Besides diagnostic applications, NP formulation strategies have also focused on therapeutic delivery. The original application of nanomedicines was to deliver anticancer drugs or proteins to achieve better therapeutic effects.[2,134] With the development of gene therapy over the past decade, genetic agents have become commonly formulated drugs that can be delivered by nanovectors.[31]

The motivation to develop nanovector-assisted delivery systems is to overcome the common disadvantages of conventional chemotherapy and gene therapy. Low molecular weight anticancer drugs have a random distribution throughout the body and usually come with negative side effects.[2] Additionally, some drugs like paclitaxel have very poor solubility in aqueous solution. Gene therapy agents, such as pDNA and siRNA, are not stable in the blood stream due to degradation by nucleases and thus have short biological halflives.[135] Encapsulation of drugs by polymer platforms can greatly improve the drug solubility and alter the biodistribution of these anticancer agents by extending their blood circulation time and assisting in their accumulation at the tumor through both active and passive targeting, such as the EPR effect.[39,112] Furthermore, the unwanted side effects caused by chemotherapeutics can be minimized due to their better biodistribution and controlled release from non-toxic polymers. Gene therapy cargos can also be protected from enzymatic degradation and random protein absorption.[67,68] In addition, active targeting moieties can also be built into the nanovectors in order to achieve even better therapy efficacy by improved targeting to solid tumors.[87,96,136]

On a more complex level, nanomedicines are able to cross bio-barriers that are difficult for conventional chemotherapy and gene therapy agents. At the tissue and organ level, the BBB is considered the main obstacle that blocks effective therapy for brain tumors. NPs with proper surface coating can assist drugs in crossing the BBB. For instance, NPs coated with polysorbate 80 or glutathione have been shown to improve chemotherapeutic delivery for brain cancer treatment.[137,138] Bio-barriers also exist on the cellular level. For example, clathrin-mediated endocytosis usually results in endosomal and lysosomal entrapment where the acidic environment (pH 4.0–6.5) leads to degradation of genetic agents and the detoxification of chemotherapeutics.[139-141] One solution to this problem is to alter the uptake pathway of the nanomedicine by introducing receptors for the cavoline-mediated pathway.[140,142] Considering the difficulty in maintaining the bioactive function of ligands on the nanomedicine surfaces due to the effect of protein coronas, an alternative is to design endosomal and lysosomal escapable systems that can relocate the therapeutic payloads back to the cytosol and allow nuclear localization. [143-145]

Another advantage of nanomedicine-assisted drug delivery is that the drug release profile can be tailored by tuning the composition of the NPs or by adding a stimulus-responsive property to the system. Diffusion-controlled delivery means controlling the drug release through the chemical or architectural design of the nanovectors. For example, it is commonly believed that a NP with strong hydrophobic core interactions with the drug cargo tends to have slower

release of hydrophobic cargos. The release kinetics can therefore be tailored by carefully altering the hydrophobic to hydrophilic ratio of the polymer system. For triggered drug release, the most common strategy is to design a pH-responsive system. The idea of this strategy is based on the fact that pH values between healthy tissue (pH 7.4) and tumor tissue (pH 6.5-7.2) are different.[146] Nanocarriers can be designed to have low or no drug release at pH 7.4 but rapid drug release at lower pHs. Besides the pH responsiveness, other exogenous stimuli-responsive nanomedicines have been designed that show sensitivity to changes in temperature, magnetic field, light, and ultrasound.[147-150]

In addition, NPs can also help to overcome multidrug resistance. This can be achieved via the intrinsic physical chemical properties of the NP[151] or by co-delivery of chemotherapeutics and siRNA that inhibit the overexpression of p-glycoprotein on cancer cells.[152]

1.3.5 Theranostic systems

Recently, nanomedicines with both diagnostic function and drug delivery capability have become the focus of intense research activity. Such nanoscale systems are called theranostic NPs where the term 'theranostic' is derived from the combination of the words 'therapy' and 'diagnostic'.[153] The primary goal of theranostic devices is to enable detection and treatment of diseases in a single procedure.[113] Such systems provide a powerful and non-invasive approach to tracing drug delivery, monitoring drug release, and assessing drug efficacy.[154]

Most types of NPs used in imaging or drug delivery applications can be redesigned as theranostic platforms. Thermally cross-linked superparamagnetic iron oxide nanoparticles (TCL-SPIONs) with carboxyl groups in the polymer coating layers can incorporate DOX via electrostatic interactions. The resulting DOX–TCL-SPION enables the delivery of DOX to tumors along with the detection of tumors by MRI.[155] Besides imaging payloads and drugs, targeting moieties can also be integrated to facilitate targeted delivery. For instance, magnetic IONPs conjugated with the amino-terminal fragment peptide can perform targeted delivery of gemcitabine to pancreatic cancer in mice and can generate detectable MRI signals during the process.[156] Furthermore, multimodal imaging and therapy can also be achieved. A PEGylated nanocomplex with biotinylated antibodies has been shown to be capable of mediating MRI and near-infrared fluorescence imaging while providing photothermal therapy functionality.[113]

Recently, fluorinated polymer NPs have been considered as a promising approach to developing theranostic NPs due to their ability to generate ^{19}F-MRI signal which has few interference signals *in vivo* and to allow the possibility to tailor the drug-release profile.[83] The third paper in this thesis focused on the development of such polymer systems and evaluated them as theranostic systems *in vitro*.

1.4 POLYMER-BASED ANTITUMOR NANOMEDICINE

Polymer-based nanomedicine refers to non-viral nanovectors that contain polymers such as polymer-inorganic hybrids, polymer-drug conjugates, polymer-protein conjugates, polyplexes, and polymer micelles.[157] Common properties of successful polymer-based nanomedicines for anticancer applications are that they 1) are all water-soluble; 2) can improve the solubility of insoluble anticancer agents; 3) are non-toxic or only slightly toxic to healthy tissue; 4) can evade the immune system; 5) have long blood circulation times; and 6) can enhance the bioavailability of therapeutics or imaging payloads at tumor sites.[157] Based on the research in this thesis, two types of polymer nanomedicines are introduced below.

1.4.1 Dendritic polymer systems

Most polymer-based nanomedicines currently approved for clinical use have linear polymer architectures. However, significant efforts have been put into the development of polymer nanomedicines with more complex architectures such as dendritic polymer systems. Two kinds of dendritic polymers – dendrimers (including dendrons) and hyperbranched polymers – are commonly used in anticancer research (Figure 4 A). Dendrimers and dendrons are perfectly branched dendritic polymers with well-controlled size, shape, and molecular weight and show monodispersity.[158,159] They are usually synthesized from either the divergent approach (from the inside out) or convergent approach (from the outside in) via multi-step reactions.[160] The resulting macromolecules have a central core bound to repeating units that form layer-like structures. Each layer of the repeating units is called one 'generation'. Based on the number of generations and the chemical composition of the repeating units, the number of terminal groups on the outside layers can be determined.

Compared to dendrimers and dendrons, hyperbranched polymers can be more quickly and easily produced via one-step polymerization from ABn monomers ($n \geq 2$).[161] However, the resulting hyperbranched polymers are structurally imperfect because of the occurrence of linear chains due to random competitive reactions during the synthesis.[160] Therefore, hyperbranched polymers do not have a real 'generation' number like dendrimers and dendrons, and the term 'pseudo generation' is usually applied to describe the statistical 'generation' of hyperbranched polymers.[162]

Both dendrimers (dendrons) and hyperbranched polymers have been investigated as candidates for anticancer treatment. For example, polyamidoamine (PAMMA) dendrimers have been used in DNA or siRNA delivery due to their cationic property.[69,163] More recently, poly-2,2-bis(methylol) propionic acid (bis-MPA)–based hyperbranched polymers demonstrated good potential in drug and gene delivery because of their non-toxic and biodegradable properties.[164,165] In addition, one of their derivative structures – dendritic linear (DL) (or linear dendritic) hybrids (Figure 4B) that usually consist of a dendron head and a linear polymer tail – has also been investigated and shown to have promising features

as a drug or gene delivery system.[166-168]

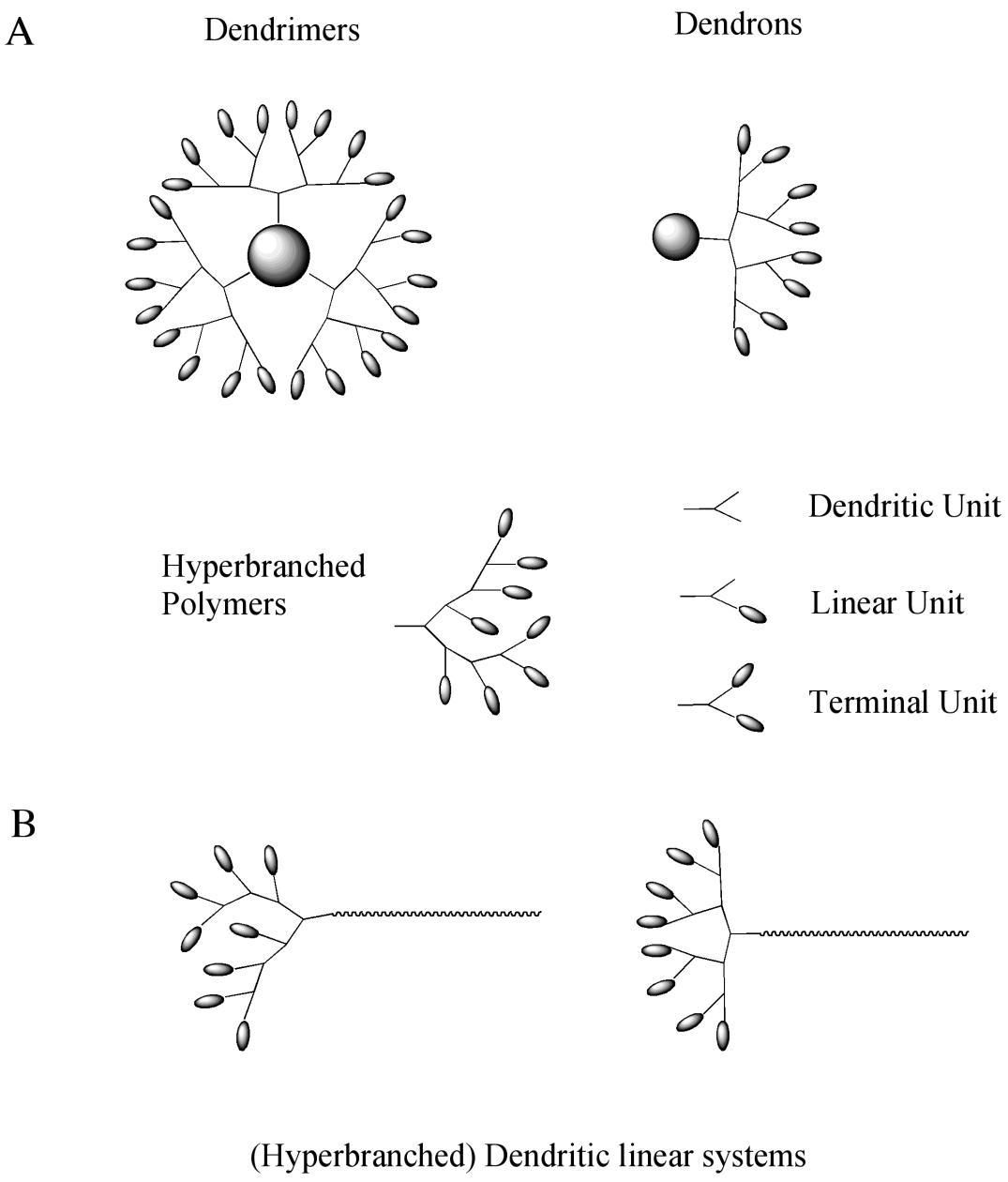

Figure 4. Dendritic polymers in biomedical applications. Structures of A) dendrimers, dendrons, and hyperbranched polymers and B) dendritic-linear polymers.

1.4.2 Unimolecular polymer NPs

The increased interest in developing polymer-based unimolecular micelles as nanovectors comes from the instability of copolymer micelles *in vivo*. Amphiphilic copolymers can self-assemble into micelles, which have a typical core-shell structure consisting of a hydrophobic core and a hydrophilic surface (shell). Polymer micelles have been investigated as desirable carriers for imaging and therapeutic payloads because they have high loading capacity,

increased solubility of hydrophobic drugs, and the ability to evade RES clearance and to increase the EPR effect.[169] However, the use of classical multi-molecular micelles is hindered by their intrinsic limitation regarding the structural stability of the micelles. Block copolymer micelles can only maintain their structure above the critical micelle concentration (CMC), otherwise they will disassemble.[170] Most NPs for antitumor applications are administered through intravenous injection leading to unavoidable dilution in the bloodstream that can cause disassembly and burst release of the cargo.[79,171] In order to overcome the CMC issue, Wooley *et al.* introduced the 'shell cross-linked' concept to enhance the stability of polymer micelles *in vivo*.[77,172,173] An alternative approach is to develop core-shell type unimolecular micelles formed from a single polymer macromolecule. One strategy is to construct dendrimers or dendrons with controlled molecular weight, size, and shape; however, the multi-step synthesis of such molecules is tedious and time consuming.[158] Hyperbranched block copolymers can be designed as unimolecular macromolecules by covalently binding hydrophilic polymers such as PEG to the hydrophobic dendritic core via chain extension. The covalent linkage between the core and shell imparts the micelles with excellent stability, and the synthesis procedure is less time consuming compared to dendrimers.[171,174] In **paper IV**, we developed a library of such polymers and explored them as DDSs.

1.5 LIPOPROTEIN-BASED NANOPARTICLS

Although 'nanoparticles' is a relative new word, naturally occurring NPs have always been present inside us. The idea of using liposomes as artificial delivery vectors is actually inspired by the structure of the cell membrane, which mainly consists of a double layer of phospholipids and various kinds of proteins. There is one type of endogenous NP in our body, called lipoprotein, that is very similar to the cell membrane and consists mainly of proteins and phospholipids.[140] Lipoproteins transport hydrophobic cholesterol among cells from different organs via the circulatory system.[175] As a natural substance in the body, there is no biocompatibility issue for lipoproteins. Furthermore, they have a hydrophobic core that can encapsulate hydrophobic molecules through reconstitution, and the hydrophilic surface allows further modifications to generate multifunctional NPs.[175-178] Therefore, efforts have been made to produce artificial lipoprotein mimics for diagnostic and therapeutic applications.[179-181] Recently, statins were reconstituted in high-density lipoprotein NPs dually labeled with gadolinium and the fluorescent dye Cy5.5 that allow both MRI and near infrared fluorescence imaging tracking. Both *in vitro* and *in vivo* analysis showed that the NP could inhibit inflammation in atherosclerotic plaques.[182] A lapatinib-incorporated lipoprotein NP has also been studied as a breast cancer treatment.[183] In **paper VI**, we proposed a new type of lipoprotein-like NP, called salipro-NP, that consist of saposin A and hydrophobic phospholipid-containing substances. Such NPs were evaluated as a DDS and a potential vaccine carrier.

1.6 NPS IN DIFFERENT PAPERS

In this thesis, several polymer based NPs and one lipoprotein like NP system were investigated. The differences among these systems and the significant of study in each paper are summarized in Table 3.

Table 3. NPs involved in this thesis.

Paper NO.	Description of NPs	Significance
I	Hyperbranched dendritic linear polymer micelles *vs.* dendrons dendritic linear polymer micelles	Hyperbranched polymer can be produce in large scale
II	Hyperbranched copolymer micelle with Boltorn (polyester) core and PEG tails	Uptake mechanism of hyperbranched polymer NPs
III	Fluorinated copolymer micelles with different structures of the hydrophobic core	Theranostic systems, allow ^{19}F-MRI imaging and drug delivery
IV	Unimolecular micelles with hyperbranched cores	Eliminate CMC issue
V	Histamine functionalized block copolymer micelles	Endo-lysosomal escape property
VI	Lipoprotein NP, consisted of saposin A and phospholipids	Multifunctional, including drug delivery and antigen carrier (NP based vaccine)

2 AIM OF THE THESIS

The overall aim was to develop NP carriers as drug delivery platforms for breast cancer treatment. The specific aims of the studies within this thesis were to:

1. Establish a method to develop hyperbranched linear polymers and to determine their capability as a DDS compared to dendrimers.
2. Investigate the cellular uptake mechanism and intracellular trafficking pathway of bis-MPA–based hyperbranched polymers.
3. Develop a multifunctional theranostic NP system that can deliver DOX and allow for imaging via ^{19}F-MRI signals.
4. Develop unimolecular polymer NPs to avoid CMC problems and to evaluate them as a DDS.
5. Evaluate the effects of histamine modification on polymer NPs to design NPs with endolysosomal escape capabilities.
6. Design and develop a bio-derived multi-functional NP system that can delivery various molecules.

3 MATERIALS AND METHODS

3.1 MATERIAL SYNTHESIS

The detailed synthetic procedures can be found in **papers I–V**. The expression and purification of saposin A, bacterial peptide transporters POT1 and POT2, and human membrane protein Synaptophysin as well as the generation of salipro particles are described in detail in **paper VI**.

3.2 CHARACTERIZATION OF POLYMERS

3.2.1 Size exclusion chromatography (SEC)

In **papers I, III, and IV**, SEC (Dimethylformamide, DMF) was performed with a TOSOH EcoSEC HLC-8320GPC system equipped with an EcoSEC RI detector and three columns (PSS PFG 5 μm, Microguard 100 Å, and Microguard 300 Å) from PSS GmbH. The mobile phase was 0.2 $mL \cdot min^{-1}$ DMF with 0.01M LiBr, and the system was run at 50 °C and calibrated with narrow linear poly(methyl methacrylate) standards using a conventional calibration method. Corrections for flow-rate fluctuations were made using toluene as an internal standard. PSS WinGPC Unity software version 7.2 was used to process the data.

In **paper I**, SEC ($CHCl_3$) was performed with a Verotech PL-GPC 50 Plus system equipped with a PL-RI detector, and two PLgel 10 μL mixed (300 × 7.5 mm) columns from Varian were used. The mobile phase was 1 $mL \cdot min^{-1}$ $CHCl_3$, and the system was calibrated with polystyrene standards.

For the detailed method of size exclusion chromatography–multiple angle laser light scattering (SEC-MALLS), please see **paper IV**.

3.2.2 Matrix-assisted laser desorption/ionization time-of-flight (MALDI-TOF)

A Bruker UltraFlex MALDI-TOF MS with a SCOUT-MTP Ion Source (Bruker Daltonics, Bremen) was used with a N_2 laser (337 nm) and reflector design. SpheriCal® calibrants were used to calibrate the instrument, and the resulting spectra were analyzed with the FlexAnalysis software version 2.2 from Bruker Daltonics.

3.2.3 Critical micelle concentration (CMC)

The CMC of micelles in PBS solution was determined by fluorescence spectroscopy (Varian Cary Eclipse) by collecting emission spectra using an excitation wavelength of 332 nm at room temperature.

3.2.4 Nuclear magnetic resonance (NMR)

A Bruker Avance 400 MHz NMR instrument was used to record ^{1}H-NMR and ^{13}C-NMR (1D) spectra for structure analysis. $CDCl_3$, $(CD_3)_2SO$, D_2O or MeOD were used as the solvent, and the residual solvent peak was used as the internal standard.

The detailed methods of ^{1}H NMR and ^{19}F-NMR diffusion can be found in **papers I and III**.

3.3 PREPARATION OF NPS AND DRUG-LOADED NPS

Polymer-based NPs were prepared via a two-phase emulsion method. A certain amount of polymer was dissolved in PBS and mixed with 1 mL organic solvent ($CHCl_3$ or CH_2Cl_2). Polymers self-assembled into NPs after the evaporation of the organic solvent while stirring overnight. DOX-encapsulated NPs (DOX-NPs) were prepared in a similar way by mixing DOX dissolved in organic solvent with the polymer dissolved in PBS solution. DOX-NPs formed after the evaporation of organic solvent while stirring overnight. Free DOX was removed by spin filtration with a molecular weight cut-off (MWCO) of 3 kDa. The concentration of DOX in the NPs was measured by comparing UV absorbance at 490 nm of samples diluted with DMF:H_2O (4:1) to a standard curve (five replicates).

In **paper VI**, daunorubicin was incorporated into salipro-NPs by first mixing daunorubicin stock solution with brain-lipid solution and then adding saposin A to the system. The mixture was incubated for 10 min at 37 °C then purified with a HiLoad SuperdexTM 200 16/60 GL column using an ÄKTA Explorer TM 10 chromatography system (both from GE Healthcare). UV absorbance was measured at 280 nm (protein) and at 480 nm (daunorubicin). The concentration of incorporated daunorubicin was determined by comparing UV absorbance at 488 nm using a UV spectrometer (NanoDrop ND1000, Thermo Fischer) to daunorubicin standard curves. Detailed information on this procedure and the methods of incorporation of other molecules are described in **paper VI**.

3.4 CHARACTERIZATION OF NPS

3.4.1 Transmission electron microscopy (TEM)

The morphology and dry size of NPs (**papers III, IV, and V**) were observed via TEM. For the polymer NPs, 3 μL each of NP or DOX-NP (*ca.* 50 $\mu g \cdot mL^{-1}$ in PBS) was added and kept for 20 seconds on a glow-discharged, carbon-coated Formvar grid (Electron Microscopy Sciences). The liquid sample was removed and the grid was stained with 2% (w/v) aqueous uranyl formate solution for another 20 seconds. TEM images were obtained with an FEI Morgagni 268(D) Transmission Electron Microscope at 80 kV at 44,000× magnification.

3.4.2 Dynamic light scattering (DLS) and zeta potential

The hydrodynamic size and surface charge of NPs were measured with DLS and zeta potential, respectively, with a Malvern Zetasizer NanoTZ. Samples were measured at 25 °C or 37 °C in filtered PBS. Polymer NPs were analyzed at a concentration of 0.25 $mg \cdot mL^{-1}$, and salipro particles were measured at 1.0 $mg \cdot mL^{-1}$. DOX-NPs were evaluated directly after the removal of free DOX. Each sample was measured by running 10 scans, and at least three parallel measurements were performed.

3.4.3 *In vitro* ^{19}F-MRI

The ^{19}F-MRI analysis of NPs was conducted with an MR-400 scanner (Varian Inc, Yarnton, UK). NPs (10 $mg \cdot mL^{-1}$ in PBS) were loaded into plastic syringes (d = 6 mm) and placed in a fixed-tune surface coil with a curved housing designed for mouse head ^{19}F-MRI (Rapid Biomed, Rimpar, Germany). Images were acquired by employing a gradient echo sequence with tr and te of 200 ms and 1.66 ms, respectively, and a flip angle of 20°. The matrix size was set as 64 × 64 mm^2 equivalent to 48 × 48 mm^2 for a slice thickness of 4 mm.

3.5 *IN VITRO* DRUG RELEASE

The drug release property of different NP systems was evaluated in a buffer system *in vitro*. In **papers I, III, IV, and V**, 3 mL of free DOX or DOX-NPs were loaded into dialysis cassettes (MWCO 3,500, Slide-A-Lyzer G2, Thermo) and suspended in 4 L of PBS (pH 7.4, pH 6.0 for **paper V**) solution with magnetic stirring at 37 °C. Aliquots of 10 µL sample (triplicates) from the inside of the cassettes were collected at 0, 2, 8, 10, 12, 24, 48, and 72 h and transferred into 96-well fluorescence plates. A total volume of 100 mL DMF in H_2O (4:1) was added to each sample to disaggregate the NPs, and the fluorescence intensity was determined with a multi-mode microplate reader (BioTek Synergy™ MX) at the wavelength of 485/595 (excitation/emission) nm.

In **paper VI**, 35 µL of free daunorubicin or daunorubicin-incorporated NP solutions were loaded into dialysis units (Slide-A-Lyzer, Thermo) and suspended in 1 L PBS (pH 7.4) at 37 °C with magnetic stirring. Aliquots of 10 µL (triplicates) were collected from the inside of the units at 0, 4, 12, 24, 48, and 72 h. A total volume of 100 mL of DMF in H_2O (4:1) was added to each sample to disaggregate the NPs, and the fluorescence intensity was determined with a multi-mode micro plate reader (BioTek Synergy™ MX) at the wavelength of 485/595 (excitation/emission) nm.

3.6 CELL-BASED EXPERIMENTS

3.6.1 Cell lines

Human breast cancer cell lines MDA-MB-231, MDAMB-468, and MCF-7 were purchased from American Type Culture Collection (ATCC), and the mouse monocyte macrophage cell line RAW 264.7 was obtained from Prof. Agneta Richter-Dahlfors, Karolinska Institutet. Cells were maintained with complete Dulbecco's modified Eagle medium (DMEM) (pH 7.4) supplemented with 10% (v/v) fetal bovine serum (FBS), 100 $U \cdot mL^{-1}$ penicillin-streptomycin, and 2 mM glutamine solution at 37 °C with 5% CO_2. Breast cancer cells were harvested by trypsin, and RAW 264.7 cells were harvested by scraping.

3.6.2 3D cell models

3D spheroid models were established with MDA-MB-231 cells by adapting the methods described by Heuchel *et al.*[184] Briefly, cells were harvested, washed, and seeded onto 96-well plates (round bottom) at a concentration of 3000 cells/100 mL DMEM medium (phenol red-free, supplemented with 20% methylcellulose). Cells were cultured at 37 °C for 48 h for the formation of 3D spheroids.

3.6.3 3-(4,5-dimethylthiazol-2-yl)-2,5-diphenyltetrazolium bromide (MTT) assays

Cellular mitochondria function was measured by MTT assays. Cells were harvested and seeded into 96-well plates at a concentration of 5×10^4 cells/well (in 100 μL DMEM) and cultured for 24 h. The medium was replaced with 100 μL of fresh medium containing various concentrations of NPs, DOX-NPs, or DOX (4 or 5 parallel wells for each concentration). A total volume of 10 μL of MTT solution (5 $mg \cdot mL^{-1}$) was added to each well after 12, 24, 48, or 72 h and then 100 μL sodium dodecyl sulfate (SDS) solution (10%) was added to stop the assay. The absorbance was measured after an additional 18 h in a plate reader at 570 nm. (BioTek Synergy™ MX) (**Papers I–V**)

3.6.4 ATP luminance viability assay

In **paper V**, the viability of MDA-MB-231 cells in 2D and 3D culture were also evaluated via CellTiter-Glo Luminescent Cell Viability Assay (Promega). Briefly, 3D spheroids or 2D cultures in 96-well plates were incubated for 72 h in 200 mL of DMEM medium (phenol red free) containing NPs (0.1–100 $\mu g \cdot mL^{-1}$), DOX, or DOX-NPs (0.01–10 $mg \cdot mL^{-1}$). Six replicates were set for each sample concentration. A total of 120 mL of medium was removed carefully (to avoid loss of spheroids), and 80 mL of CellTiter-Glo Luminescent reagent was added to each well. Plates were shaken gently in the dark for 20

min. The mixtures from each well were then transferred into white 96-well plates, and the resulting luminescence was quantified with an Infinite F200 plate reader.

3.6.5 Apoptosis assays

Cells were seeded on 6-well plates at a concentration of 5×10^5 cells per well and pre-cultured for 24 h before treatment. Cells were treated with designated amounts of DOX, DOX-NPs, or NPs for 12, 24, 48, or 72 h (see **papers III and V**). Cells were then harvested and washed with PBS twice and stained with fluorescein isothiocyanate (FITC)-labeled Annexin V and propidium iodide (PI). Samples were analyzed with either a FACSCalibur (BD Science) (**paper III**) or an Accuri C6 (BD Science) (**paper IV**) flow cytometer by collecting 10,000 events. FITC fluorescence was excited by the 488 nm laser and collected on the FL-1 (533/30 nm) detector, and PI signal was collected on the FL-3 (>670 nm) detector. Data were analyzed using the CellQuest and BD Accuri C6 Analysis software, respectively.

3.6.6 Quantitative cellular uptake analysis

In **paper II**, the cellular fluorescence was quantified as the fluorescent intensity normalized to milligrams of cell protein. Cells were seeded on 12-well plates at a concentration of 2×10^5 cells per well and pre-cultured for 24 h. Cells were then treated as follows. For the concentration-dependent assay, cells were treated with 0–300 $\mu g \cdot mL^{-1}$ of NPs for 3 h. For the time-dependent assay, cells were treated with 300 $\mu g \cdot mL^{-1}$ of NPs for 1, 2, 4, 6, 12, or 24 h. For the temperature-dependent assay, cells were treated with 300 $\mu g \cdot mL^{-1}$ of NPs for 3 h at 37 °C or 4 °C. For the serum-dependent assay, cells were treated with 300 $\mu g \cdot mL^{-1}$ of NPs for 3 h with or without serum. For the endocytotic inhibition assays, cells were incubated with inhibitors first (for details see **paper II**), then washed and treated with 300 $\mu g \cdot mL^{-1}$ of NPs for 3 h. After treatments, cells were lysed in 100 μL of cell lysis buffer for 15 min. Then 10 μL of cell lysate was used to quantify the protein amount using a BCA assay, and the fluorescence of the remaining lysate was measured by a multi-mode microplate reader (BioTek Synergy™ MX) at a wavelength of 490/520 (excitation/emission) nm.

In **paper III**, cellular uptakes of NPs and DOX-NPs were compared using a flow cytometer. Cells (5×10^5) were seeded, treated with 5 $\mu g \cdot mL^{-1}$ DOX or DOX-NPs and 100 $\mu g \cdot mL^{-1}$ FITC labeled NPs (FITC-NPs), washed, and harvested as in the apoptosis assay. Cells were re-suspended in 0.5 mL of PBS for immediate analysis by a FACSCalibur (BD Science) flow cytometer collecting 10,000 events. The fluorescence of the FITC-NPs was excited by the 488-nm laser and collected in the FL-1 channel (530/30 filter/bandpass), and DOX fluorescence was excited by the 635-nm laser and collected in the FL-4 channel (661/16 filter/bandpass). Data were analyzed using the CellQuest software.

3.6.7 Intracellular tracking of NPs (confocal microscopy)

For 2D cell cultures, cells (5×10^5 cells/well in **papers II, III, IV, and VI** and 1×10^5 cells/well in **paper V**) were seeded on 6-well or 12-well plates with coverslips at the bottom (**papers II, III, and VI**) or on glass-bottom dishes (P35G-0-10-C, MatTek, in **paper V**) and pre-cultured for 24 h. Cells were then treated with samples at the designated concentrations for different periods of time (details are in the respective papers). Cells were washed and stained with fluorescent dyes before or after being fixed with 4% formaldehyde (details in the papers). For live-cell imaging, no fixation was required. Cells on the slides were washed and sealed with mounting medium. Fluorescence was observed with either a FV1000 Olympus confocal microscope (**papers II, III, and VI**) or a Zeiss LSM 510 Meta confocal microscope with a temperature control chamber (**paper V**). For detailed laser settings, please see **papers II–VI**. Images were acquired with FV1000 software (FV10-ASW) or LSM software, and co-localization was analyzed with the ImageJ software.

For 3D cell cultures, spheroids were obtained as described in the cell models section. The spheroids were then incubated for 4 h in 2 $mg \cdot mL^{-1}$ of DOX or DOX-NPs. The spheroids were transferred into Eppendorf tubes and gently spun for 15 s. The supernatant was removed, and fresh PBS was added. The washing step was repeated three times. Cells were stained with Hoechst (5 $mg \cdot mL^{-1}$), and LysoTracker Deep Red (100 nM) or MitoTracker Deep Red FM (100 nM) was then added and incubated for another 15 min. Spheroids were washed another three times then carefully suspended on glass-bottom dishes (P35G-0-10-C, MatTek). A Zeiss LSM 510 Meta confocal microscope with a temperature control chamber was used to observe the samples. Detailed settings can be found in **paper V**. Data were collected with the LSM software, 3D images were reconstructed with the Imars software, and co-localization was analyzed with ImageJ.

3.7 STATISTICAL ANALYSIS

All the quantitative data from DLS, viability assays, drug release assays, and apoptosis/necrosis analysis are presented as mean values with standard deviations (SD). Statistical analysis was performed via ANOVA followed by a post hoc test (Tukey HSD, alpha 0.05) using KaleidaGraph v4.1 (Synergy Software, Reading, PA).

4 RESULTS

4.1 PAPER I. SIDE BY SIDE COMPARISON OF DENDRITIC LINEAR HYBRIDS AND THEIR HYPERBRANCHED ANALOGS AS MICELLAR CARRIERS OF CHEMOTHERAPEUTICS

Hydrophilic DL hybrids can form micelles in aqueous environments and have been shown to be promising in drug delivery applications.[185] However, the synthesis of the dendron components involves multiple steps, and the procedure is very time consuming.[158] Thus the use of DL hybrids as a DDS has been hindered by the difficulty in producing large amounts of material.

To solve this problem, we focused our efforts on developing a novel method for the rapid and large-scale synthesis of DL hybrids. The resulting DL hybrids are hyperbranched DL hybrids (HBDL), which were synthesized via Fisher esterification reactions of bis-MPA starting from a monomethylether linear PEG (mPEG, MW 5000 $g \cdot mol^{-1}$) in one step. These HBDL were further compared to their perfect DL analogs produced through copper(I)-catalyzed azide–alkyne cycloaddition (CuAAC)-based click chemistry.

HBDL hybrids of the second (DL PEG-[HBG2]-$(OH)_4$) and third pseudo-generation (DL PEG-[HBG3]-$(OH)_8$) were first synthesized using mPEG and bis-MPA monomers via Fisher esterification reaction on a 50 g scale. They were then end-capped with the addition of a layer of bis-MPA monomers to their hydroxyl groups. Benzylidene decoration was then introduced to the final layer of bis-MPA to increase the hydrophobicity of the system for further drug encapsulation. The resulting HBDL hybrids – DL PEG-[HBG3]-$(Bz)_4$ and DL PEG-[HBG4]-$(Bz)_8$ – were further examined by ^{1}H-NMR and SEC to confirm their structural integrity, and their degree of branching was calculated from ^{13}C-NMR measurements.[186] The perfectly branched DL with benzylidene decoration in generation three (DL PEG-[G3]-$(Bz)_4$) and four (DL PEG-[G4]-$(Bz)_8$) were synthesized via CuAAC click chemistry[187] by clicking mono PEG_{5k}-acetylene to Azide-[G3]-$(Bz)_4$ or Azide-[G4]-$(Bz)_8$. The structural integrity and perfection were confirmed by ^{1}H-NMR and MALDI-ToF MS, respectively.

In the next step, we obtained micellar NPs and DOX-NPs via the two-phase emulsion method, and the size of NPs/DOX-NPs was determined by DLS. DL micelles tended to have smaller size compared to HBDL micelles with the same (pseudo) generation according to number-averaged DLS. After DOX loading, the size of the micelles increased significantly and aggregation was found for DOX-HBDL NPs indicating insufficient stealth or steric repulsion from PEG segments. Further study on drug release in a PBS system showed a burst release (80% of the DOX was released within 12 h) of all four materials suggesting that the hydrophobic compartment was not large enough to effectively transport the drug.

To further evaluate the biocompatibility of HBDL and DL micelles and the efficacy of DOX-loaded NPs, we performed MTT assays to measure the mitochondrial function of the

MDA-MB-231 breast cancer cell line. Mitochondrial activity was higher than 90%, so both the DL and HBDL micelles were considered to be non-toxic to MDA-MB-231 cells in the range of 0.1–100 $\mu g \cdot mL^{-1}$ after 48 h incubation. However, DOX-NPs displayed a dose-dependent toxicity against the cells over the same incubation time. Significantly lower mitochondrial viability was found for DL PEG-[HBG3]-$(Bz)_4$-DOX, DL PEG-[HBG4]-$(Bz)_8$-DOX, and DL PEG-[G4]-$(Bz)_8$-DOX compared to free DOX and DL PEG-[G3]-$(Bz)_4$-DOX at a DOX concentration of 10 $\mu g \cdot mL^{-1}$ (approximately equivalent to 100 $\mu g \cdot mL^{-1}$ of NPs). This indicates that HBDLs are able to enhance the efficacy of the drug.

In summary, the bis-MPA-based HBDL hybrids can be produced on a large scale and much more quickly through Fisher esterification reactions. The HBDL NPs are non-toxic and can enhance drug efficacy in breast cancer treatment. With suitable modification of PEG molecules and hydrophobic compartments, HBDL NPs are promising for drug delivery applications.

4.2 PAPER II. ENDOCYTIC UPTAKE AND INTRACELLULAR TRAFFICKING OF BIS-MPA-BASED HYPERBRANCHED COPOLYMER MICELLES IN BREAST CANCER CELLS

Dendrimers and their imperfect analogues – hyperbranched polymers – are a class of polymers with highly branched and dendritic architecture. This unique structure leads to enhanced solubility and provides a large number of available surface groups that make dendrimers and hyperbranched polymers promising as scaffold materials for tissue engineering, as DDSs, and as diagnostic imaging agents. bis-MPA-based dendrimers and hyperbranched polymers have been investigated for use in targeted positron emission tomography (PET) imaging and as carriers of DOX.[188,189] These polymers are biodegradable and display good biocompatibility towards human cancer cell lines and primary cells.[170,190]

In this study, we focused on understanding the cellular uptake and intracellular transport profiles of the Boltorn-PEG system. This system is derived from hyperbranched bis-MPA units and PEG segments and has demonstrated promising properties as a DDS.[165] We first synthesized the Boltorn-PEG system (H30-$(PEG_{10k})_5$) from the hyperbranched polyester Boltorn H30 and PEG monomers as described in previous research.[165] We then conjugated them with the organic dye fluorescein to form H30-$(PEG_{10k})_5$-FL as describe by Gong *et al.*[191], and the pure polymer was obtained via dialysis (10 kDa MWCO) and freeze-drying. The micellar NPs with an average size of 54 ± 20 nm (DLS intensity average) were formed by self-assembly of copolymers in PBS solution.

In order to understand the profile of the uptake of NPs, we first investigated the possible factors that might influence the cellular uptake of NPs using the breast cancer cell line MDA-MB468. The cellular uptake of NPs was quantified by determining the normalized florescence intensity with respect to milligrams of cell protein.

For the time-dependence investigation, we incubated cells with 300 $\mu g \cdot mL^{-1}$ of NPs (equivalent concentration of 1 μM of conjugated fluorescein) for different times. We observed a significant internalization after 30 min indicating rapid translocation of NPs into cells. The half-maximal uptake was found around 0.8 h after which the uptake amount increased continuously. The NP concentration-related uptake was then assessed by incubating cells with various concentrations of NPs from 0 to 300 $\mu g \cdot mL^{-1}$ for 3 h. Not surprisingly, a concentration-dependent behavior was observed, and the internalization of NPs was also confirmed by confocal microscopy. For the temperature (energy)-dependence assessment, cells were incubated with NPs (300 $\mu g \cdot mL^{-1}$) for 3 h at 37 °C or 4 °C, and a clear reduction of uptake was observed at the lower temperature through both quantification analysis and confocal imaging. Furthermore, we confirmed the energy-dependent uptake of NPs by administering 10 mM sodium azide and 5 mM 2-deoxyglucose to cells and observing a significant decrease in the uptake of NPs. Serum was also found to inhibit the internalization of NPs compared to normal medium without serum, indicating that the association of serum proteins to the NPs might influence the uptake profile of the NPs.

Second, the mechanisms of NP internalization were determined by co-localization studies of NPs and fluorescence-stained biomarkers of endocytic pathways. Three different endocytic pathways were investigated, including the clathrin-dependent (transferrin-Alexa 647 stained), caveolae-mediated (CTB-Alexa647 labeled), and macropinocytosis-mediated (dextran rhodamine stained) pathways. Strong co-localization was observed between NPs and the clathrin-dependent pathway and the macropinocytosis-mediated pathway. An endocytic inhibition assay was used to confirm these results. This showed significant reductions of cell-associated fluorescence in cells with inhibitors of the clathrin or macropinocytosis pathways compared to those without any inhibitors.

The last step was to identify the intracellular trafficking route of NPs after endocytosis. In order to achieve this, co-localization assessments between NPs and different fluorescence-stained organelles, such as early endosomes (EEA1), lysosomes (lysotracker), and the Golgi network (TGN), were performed with confocal microscopy after 3 h administration of NPs to MDA-MB-468 cells. Strong co-localization signal (yellow color) was observed in lysosomes, while a weak correlation was found in early endosomes and the Golgi network suggesting that the NPs were mainly trapped in lysosomes. Combined with further positive results from the study of the effects of lysosomotropic agents on the uptake of NPs, we concluded that NPs could bypass early endosomes and the Golgi network and translocate into lysosomes where they can be degraded and release their cargos.

Finally, in order to strengthen the finding of this study other cell lines including A498, MDA-MB-231, MCF-7, and RAW 264.7 were used to evaluate the uptake of NPs. These results showed very similar uptake profiles in all of these cell lines, but RAW 264.7 cells exhibited the highest level of NP internalization due to their phagocytic capacity.

In summary, bis-MPA based hyperbranched NPs can be transported into cells via clathrin- and macropinocytosis-mediated endocytosis, and the uptake process is time, concentration,

and energy dependent.

4.3 PAPER III. IN VITRO EVALUATION OF NON-PROTEIN ADSORBING BREAST CANCER THERANOSTICS BASED ON ^{19}F-POLYMER CONTAINING NANOPARTICLES

The term theranostic is derived from the combination of the words 'therapy' and 'diagnostic'. Theranostic NPs are dual-functional nanoscale systems that can serve as diagnostic agents and chemotherapeutic carriers at the same time. Fluorinated polymers can serve as imaging contrast agents for ^{19}F-MRI due to the high amount of fluorine atoms in the polymer.

To this end, a library of fluorinated NPs was developed and evaluated *in vitro* as a potential theranostic system against breast cancer cells. These NPs were obtained from the self-assembly of amphiphilic block polymers that were synthesized in a two-step strategy. In the first step, a number of different linear low molecular weight or low generation dendritic hydrophobic atom transfer radical polymerization (ATRP) initiators were synthesized via standard base-catalyzed esterification reactions. The second step was the polymerization of hydrophilic copolymers using the hydrophobic ATRP initiators from the first step and monomers of oligo(ethylene glycol) methyl ether methacrylate (OEGMA, average molecular mass (M_n) = 475) and TFEMA. The fluorine atoms (from TFEMA) were randomly introduced into the hydrophilic segments of the polymer in this step and subsequently formed either linear or star-shaped (generation zero ([G#0]), 4 arms or 16 arms) amphiphilic polymers with different molecular weights for the hydrophilic segment. The structural integrity of these copolymers was subsequently confirmed by ^{1}H-NMR and SEC analysis. All of the resulting copolymers demonstrated good solubility in PBS, very low CMCs (0.8–3.8 $\mu g \cdot mL^{-1}$), and the ability to self-assemble into NPs and to encapsulate DOX to form DOX-NPs via the two-phase emulsion method. DLS and TEM were used to confirm NPs/DOX-NP formation and to determine their diameters. TEM images revealed that NPs have circular shapes ranging in size from 7 nm to 15 nm, and this is slightly larger compared to the sizes of NPs in PBS determined by DLS (6–9 nm).

According to DLS, the sizes of DOX-NPs increased significantly after encapsulation of DOX to 800–1400 nm indicating the formation of aggregates after drug loading. In order to eliminate aggregation, the Chol-P(OEGMA-*co*-MMA-*co*-TFEMA) NP (poly(), P(); cholesterol, chol; methacrylic acid, MAA) was synthesized by replacing 50% of the OEGMA monomers with MAA monomers to provide negative charges to the NPs. The sizes of these DOX-loaded NPs were successfully reduced to 40 nm. This indicates that the aggregation of drug-loaded NPs could be reduced by introducing negative charges into the hydrophilic segments of the NPs.

Three NPs – EBiB-P(O-*co*-T), Chol-P(O-*co*-T), and [G#0]-P(O-*co*-T)$_{28k}$ – were selected for ^{19}F-NMR diffusion studies in PBS, complete DMEM, and plasma. The sizes of NPs (5.6–6.3 nm) in PBS measured by ^{19}F-NMR diffusion were very similar to the DLS results. In

DMEM and plasma, these sizes were slightly smaller than in PBS. This shrinking in size might be caused by the reduction of polymer solubility in the complex medium. However, there was no significant size increase after NPs were placed in a protein-rich environment, and this suggests that these NPs can avoid protein absorption and that the poly(OEGMA-*co*-TFEMA) provides a stealthy corona on the NPs.

To further evaluate these NPs as a DDS, their loading capacities and release profiles were also investigated. The loading efficiencies of the NPs from this library were generally similar, from 70% to 89%. In general, [G#2]-polymers displayed a higher loading capacity than [G#0]-polymers suggesting that larger hydrophobic cores have higher loading capacities. Interestingly, one of the linear core NPs, Chol-P(O-*co*-T) exhibited a similar loading efficiency(*ca.* 88%) compared to [G#2]-P(O-*co*-T)$_{23k}$ (*ca.* 89%), indicating that cholesterol is a promising candidate for constructing hydrophobic cores. For the *in vitro* drug release study, it was not surprising to find that star-like and larger hydrophobic cores displayed slower release rates and that Chol-P(O-*co*-T) showed a similar release profile compared to the [G#2]-NPs. This confirmed that [G#2]-polymers and cholesterol cores are suitable for drug delivery applications.

The efficacy and toxicity of DOX-NPs are other key properties for DDS evaluations. Cellular viability was determined by measuring mitochondrial function in cells with an MTT assay. The results revealed that pure NPs (0.01–500 $\mu g \cdot mL^{-1}$) without DOX encapsulation were non-toxic to three breast cancer cell lines (MCF-7, MDA-MB-231, and MDA-MB-468) and one monocyte cell line (RAW 264.7). However, when loaded with DOX these NPs exhibited significant toxic effects (at 10 $\mu g \cdot mL^{-1}$) towards these cell lines. They all had either similar or lower IC_{50} compared to free DOX suggesting that all of these materials have good drug-carrying properties. Apoptosis assays determined by fluorescence-activated cell sorting (FACS) also revealed that DOX-NPs could induce apoptosis in these cell lines in a similar manner as free DOX after 24 h and 48 h.

The uptake of the NPs was also confirmed by FACS showing increased FITC signals from two fluorescent labeled copolymer FITC-Chol-P(O-*co*-T)$_{15k}$ and FITC-[G#0]-P(O-*co*-T)$_{28k}$.To further track the intracellular locations of NPs, MDA-MB-231 and RAW 264.7 cells were incubated with FITC-[G#0]-P(O-*co*-T)$_{28k}$ NPs for designated time periods and observed with a confocal microscope. The FITC-NPs were mainly observed in the cytoplasm and closely surrounding the nuclei, unlike DOX or DOX released from NPs that was mainly found in the nuclei. This result confirmed the uptake of the NPs and suggested that NPs cannot penetrate the nuclear membrane. Moreover, in order to analyze the intracellular distribution of DOX release from NPs, MDA-MB-231 and RAW 264.7 cells were treated with 5 $\mu g \cdot mL^{-1}$ equivalent free DOX (control), DOX-[G#0]-P(O-*co*-T)$_{28k}$, or DOX-Chol-P(O-*co*-T) NPs for different time periods. A rapid uptake (4 h) of free DOX and DOX release from NPs was observed in these cells, and the DOX tended to concentrate in the nuclei. In addition, the signal of DOX release from the NPs became stronger from 4 h to 48 h incubation indicating that the NPs could continuously release encapsulated DOX

intracellularly.

The imaging function of the fluorinated NPs was analyzed *in vitro* by ^{19}F-MRI. The strong MRI phantoms of NPs (190–970 μM in PBS, equivalent fluorine concentrations 23–56 mM) can be rapidly achieved within 10 min scanning time. This indicated that excellent MRI signals were introduced by fluorinating the NPs and demonstrates that they are promising candidates for ^{19}F-MRI imaging.

4.4 PAPER IV. TOWARD UNIMOLECULAR MICELLES WITH TUNABLE DIMENSIONS USING HYPERBRANCED DENDRITIC-LINEAR POLYMERS

Unimolecular micelles were developed from PEGylated hyperbranched dendritic-linear polymers (HBDLPs) via a versatile two-step procedure and further evaluated as a potential DDS. The first step was to synthesize hydrophobic hyperbranched macroinitiators (HBMI) from self-condensing vinyl (*co*) polymerization (SCV(C)P) utilizing ATRP. The second step was to produce hydrophilic polymers by adding hydrophilic segments to the hydrophobic HBMI through chain extension.

In the first step, two HBMIs (full name HBMI(TBBPE-*co*-BBEMA-*co*-HA)) were synthesized from the inimer 2-(2- bromoisobutyryloxy)ethyl methacrylate (BBEMA), the comonomer hexyl acrylate (HA), and 1,1,1-tris(4-(2-bromoisobutyryloxy)phenyl)-ethane (TBBPE) by employing SCV(C)P-ATRP with different ratios of these components. The resulting HBMI-1 and HBMI-2 were further characterized by ^{1}H NMR ($CDCL_3$) and SEC. The average polymer ratio of TBBPE:BBEMA:HA was calculated as 1:12:37 for HBMI-1 and 1:51:295 for HBMI-2. Further evaluation of the HBMIs by SEC with DMF as the mobile phase showed different elution times indicating a clear difference in hydrodynamic volume between HBMI-1 and HBMI-2 whose molecular weights were determined to be 3600 g·mol^{-1} and 6100 g·mol^{-1}, respectively. In addition, the estimated average degrees of polymerization of BBEMA and HA were calculated from ^{1}H NMR as 49 for HBMI-1 and 346 for HBMI-2. The average number of Br per molecule was determined as 15 and 54 for HBMI-1 and HBMI-2, respectively, by assuming one TBBPE-moiety per HBMI and high end-group fidelity.

In the second step, a library of amphiphilic HBDLPs (HBDLPs 1–5) was synthesized by chain-extending HBMIs with different lengths of P(OEGMA) segments via ATRP. In order to demonstrate that additional functionality such as imaging properties could also be achieved with this method, an additional HBDLP was synthesized by chain-extension of HBMI-2 with P(OEGMA), the fluorine-containing copolymer TFEMA, and t-BMA followed by the removal of tert-butyl groups to form MAA residues. Such copolymers have previously been reported to be able to generate detectable ^{19}F-MRI signals for imaging applications. These HBMIs-P(OEGMA)$_x$ polymers (x = 103 kDa, 473 kDa, 230 kDa, 410000 kDa, 605000 kDa from HBDLP-1 to HBDLP-25) and HBMI-P(OEGMA-*co*-TFEMA-*co*-MAA)$_{287k}$ were further characterized using DLS, ^{1}H-NMR self-diffusion, and

SEC-MALLS. SEC-MALLS determined the molecular weight of the HBDLPs to be 100–600 $kg \cdot mol^{-1}$.

HBDLP NPs were obtained by self-assembly of materials in PBS solution following the evaporation of the organic solvent CH_2Cl_2. The mean diameters (z-average) of NPs determined by DLS were 17–39 nm. The other three average parameters (number, volume, and intensity weighted diameter from DLS) were also in a similar range as the z-average. The sizes of NPs were also measured by NMR diffusion and calculated by the Stokes-Einstein equation. The average diameters determined by this method were 10–24 nm. Despite the different diameters determined with the two methods, both DLS and NMR diffusion measurements revealed an increasing correlation between diameter and P(OEGMA) extension indicating that the HBDLPs had tunable sizes using this synthesis strategy. TEM images further confirmed the size of NPs being in the range of 10–20 nm and showed that the NPs had the expected core-shell morphology. The SEC-MALLS measurements showed that the NPs had high molecular weight range (100–600 $kg \cdot mol^{-1}$) as polymers, and this indicated that these NPs had unimolecular weights.

To evaluate these unimolecular NPs as a DDS, we first loaded DOX into the NPs via the two-phase emulsion method and measured *in vitro* drug release in PBS solution. All of the NPs demonstrated the ability to encapsulate the drug and had slower release profiles compared to free DOX in PBS (60% of the drug was released from the NPs within 10 h). Furthermore, MTT assays were carried out in three breast cancer cell lines and one mouse macrophage cell line to evaluate the toxicity of the materials. No obvious toxicity was found for NPs formed from HBDLP1–5 in the concentration range of 0.1–100 $\mu g \cdot mL^{-1}$. However, a reduction in mitochondrial function was observed in cells incubated with 100 $\mu g \cdot mL^{-1}$ of the HBDLP6 NP, and this might be due to incomplete removal of copper during the synthesis. DOX-NPs demonstrated a dose-dependent efficacy in reduction of mitochondrial function in MDA-MB-468 cells after 48 h suggesting that the NPs could deliver DOX into cancer cells. This was further confirmed by localization studies with confocal microscopy showing time-dependent accumulation of DOX released from NPs in and around the nuclei.

In summary, high molecular weight HBDLPs could be produced via SCV(C)P-ATRP. They can form unimolecular micelles and are promising in drug delivery applications.

4.5 PAPER V. HISTAMINE-FUNCTIONALIZED COPOLYMER MICELLES AS A DRUG DELIVERY SYSTEM IN 2D AND 3D MODELS OF BREAST CANCER

Polymer-based NPs have been used as DDSs in anticancer research for the last decade. One issue to achieving effective drug delivery with NPs is to overcome endosomal/lysosomal entrapment so that the drugs can be transported to their targets. pH-responsive NPs have been developed in order to achieve endo-lysosomal escape due to the ‘proton sponge’ effect caused by the charged polymer under acidic conditions.

Based on this idea, a library of polymer micelles was synthesized from poly(allyl glycidyl ether)-*b*-poly(ethylene oxide) (PAGE-*b*-PEO) followed by the functionalization of histamine and octane or benzyl groups through UV-initiated thiol-ene click chemistry to obtain the pH-sensitive property. The resulting polymers were divided into four groups based on their chemical modifications and molecular weight, including the low PXGE MW and low PEO MW group (LL); the low PXGE MW and high PEO MW group (LH); the high PXGE MW and high PEO MW group (HH); and the benzyl-containing group (B). The X in PXGE refers to allyl (A), octyl (O), or histamine (H). The chemical characteristics and structures of these copolymers were further confirmed by SEC and ^{1}H-NMR (for details, see **paper V**).

NPs were formed through self-assembly of polymers in aqueous solution, and the DOX-NPs were obtained by the two-phase emulsion method. The NPs and DOX-NPs were characterized by DLS and TEM to determine their size and morphology. The sizes of NPs measured by DLS (number mean) were in the range of 16–59 nm, and this was larger compared to the diameter determined by TEM (6–20 nm). Moreover, diameter expansion of NPs after DOX encapsulation was observed as well as some aggregations. Spherical morphology was observed for NPs and DOX-NPs in the TEM images, and the low CMC (below 10 $\mu g \cdot mL^{-1}$) suggested that these NPs could be suitable for *in vivo* drug delivery.

In the next step, we evaluated the drug loading efficiency and release profile of these DOX-NPs to explore the effect of histamine modification. Similar drug loading efficiencies of 15% to 30% (w/w) were found among most of these DOX-NPs. A lower efficiency of 12% was seen for HH3, and higher efficiencies of 36% and 44% were observed for LH2 and B2, respectively. *In vitro* drug release was tested in buffer solution at both pH 6.0 and pH 7.4. Unfortunately, no obvious difference in drug release rate was found for the same DOX-NPs at the two pHs. However, DOX-NPs with 50% histamine functionalization (DOX-LL3, DOX-LH3, DOX-HH2) displayed slower drug release rates at both pHs compared to other materials from the same group, suggesting that the overall structures of these NPs could be the reason of the slower release.

Another critical issue in DDS evaluation was the toxicity of the materials and the efficacy of DOX-NPs. To this end, 2D (MCF-7, MDA-MB-468 and MDA-MB-231) and 3D (MDA-MB-231) cell cultures of breast cancer cells were established and used in toxicity evaluations. None of these NPs demonstrated toxic effects against the tested cell lines in either the 2D or 3D cultures. However, the MTT assays in the 2D cell culture showed reduction of mitochondrial function induced by DOX-NPs compared to free drug over short treatment periods of 12–24 h. DOX-LL3 (50% histamine, low molecular weight group) displayed the strongest toxicity compared to other DOX-NPs from the same group after treatment for 72 h. Apoptosis assays with FACS revealed that DOX-NPs could induce more late apoptosis than free DOX after 72 h treatment. Histamine-containing NPs also demonstrated enhanced drug efficacy in 3D cultures according to ATP luminance assays and the presence of broken spheroids.

In order to determine the mechanism behind the enhanced efficacy of DOX-NPs compared to free drug in cancer cell treatments, confocal microscopy was used to track the distribution of DOX/DOX-NPs in cell cultures. Co-localization analysis of DOX-LL3 revealed relatively strong co-localization not only in lysosomes but also in nuclei and mitochondria, indicating partial endo-lysosomal escape. To better compare the drug distribution between free DOX and DOX-NPs in various cellular locations, a heat map was made based on the calculation of the co-localization parameters. The map showed enhanced residence of DOX-LL3 in the mitochondria and reduced drug signal in lysosomes compared to free DOX. This further confirmed that DOX-LL3 was able to partly escape endo-lysosomal entrapment and to transport DOX into the nuclei and mitochondria. To further investigate the mitochondria targeting property of the NPs, another heat map was produced for mitochondria co-localizations of three NP groups in three breast cancer cell lines. The map revealed that NPs with 50% histamine functionalization (LL3, LH3, and HH2) tended to have stronger signals compared to DOX and other NPs. We also conducted a co-localization study in 3D spheroids, and the result was consistent with previous results showing that 50% histamine-modified DOX-NPs, in particularly the ones from the low molecular weight group (DOX-LL3), displayed the lowest co-localization in lysosomes indicating endo-lysosomal escape.

Based on all of these results, we conclude that histamine functionalization enables polymer NPs to escape from endo/lysosomes and that carefully adjusting the chemical ratio of the modification improves drug delivery efficacy and drug distribution.

4.6 PAPER VI. A MULTI-FUNCTIONAL NANOPARTICLE SYSTEM BASED ON A SMALL HUMAN PROTEIN

In the first part of this work, we intended to demonstrate the formation of saposin-lipoprotein (salipro) NPs through incubation of saposin A together with lipids such as phosphatidylcholine, phosphatidylglycerol, and phosphatidylserine (PS) in solution at pH 7.4. Successful generation of salipro-NPs was confirmed by SEC analysis showing a significant peak shift of the saposin A retention time after incorporation with lipids. The same method was used to generate a fluorescent salipro-NP by incorporating PS labeled with 7-nitro-2-1,3-benzoxadiazol-4-yl (NBD). The consistency between the protein absorption peak (280 nm) and the fluorescence absorption peak (470 nm) observed by SEC proved the formation of salipro-NBD-PS NPs. The homogeneity of the NPs was confirmed by gel filtration, DLS, and negative-stain electron microscopy (EM) showing 95% homogeneity and an average NP size of 6 nm. A high degree of thermostability was also confirmed by SEC analysis after repeated freeze-thaw cycles.

Satisfied that we had successfully formed salipro-NPs, several hydrophobic drugs were added during the generation of the NPs to evaluate the NPs' ability to carry drugs. Curcumin, daunorubicin, and mitoxantrone were selected because of their intrinsic UV-absorbance characteristics. Successful incorporation of these drugs was confirmed with SEC by monitoring the absorption at 280 nm (protein), 420 nm (curcumin), 480 nm (daunorubicin), and 655 nm (mitoxantrone) separately. A positive thermal responsive

behavior in drug encapsulation was identified by comparing the daunorubicin loading efficiency at 37 °C, 50 °C, and 65 °C. The maximal incorporation of daunorubicin was achieved at 65 °C, and about 95% of the drug was loaded. A pH sensitive property of salipro-NPs was also revealed by the degradation of the NPs at pH 4.75. All of these results implied that salipro-NP might serve as a DDS.

To further evaluate salipro-NP as a DDS, several *in vitro* experiments were performed. First, we tested whether salipro-NPs can interact with cancer cells. Breast cancer cells (MDA-MB-468) were incubated with fluorescently labeled salipro-NBD-PS NPs at designated concentrations and times. Both time and concentration-dependent fluorescent signals were observed. Further co-localization revealed that the NPs were primarily located in the membrane. In the second step, the release profile of daunorubicin from NPs was investigated in PBS solution. A slow and linear release rate was observed, and 20% of the drug was released from the NPs over 24 h. This was much slower compared to unloaded drug that had 100% release from a dialysis unit within 12 h. At 96 h, 70% of the daunorubicin had been released. Further investigation of intracellular drug distribution revealed a time-dependent release of daunorubicin from salipro-NPs, and daunorubicin was observed throughout the cytoplasm after 72 h incubation. This is quite different compared to free drug-treated cells in which daunorubicin only concentrated in the nuclei after 72 h. Because salipro-NBD-PS NPs were only found in the cell membrane, this suggested that daunorubicin-carrying NPs could indeed release their cargos intracellularly.

To expand the application of salipro-NPs, we explored the possibility encapsulating insoluble membrane proteins into the salipro-NPs. Both prokaryotic (bacterial peptide transporters POT1 and POT2) and eukaryotic (the human membrane protein synaptophysin, SYP) were incorporated as confirmed by SEC. The 3D structure of salipro-POT1 was reconstructed via data collected from negative-stain EM. The analysis demonstrated that salipro-NPs could be assembled flexibly due to the adaption of the saposin A-lipid system to the size of the incorporated molecules. Satisfied with the proven concept, salipro-NPs were further used to reconstitute HIV-1 spike proteins and to maintain their ability to produce potential vaccine antigens. Salipro-HIV-spikes were formed by incubating saposin A, detergent, and HIV-1 spike proteins in the viral membrane followed by rapid removal of the detergent with spin desalting columns. Blue native polyacrylamide gel electrophoresis (BN-PAGE) analysis confirmed the formation of the desired NPs, and highly specific lectin affinity chromatography was used to further purify the NPs. The final purity of the salipro-HIV-spikes was determined by sodium dodecyl sulfate polyacrylamide gel electrophoresis (SDS-PAGE) and visualized by negative-stain EM. The function of salipro-HIV-spikes was further determined by the binding of PG16 antibody.

5 GENERAL DISCUSSION

5.1 DRUG LOADING AND RELEASE FOR POLYMER NPS

In **papers I and III–V**, drug loading was mainly achieved via a two-phase emulsion method based on the hydrophobic entrapment of the drugs.[192,193] The loading efficiency was in the middle range compared to previously published reports with the same method.[165,168] The fundamental advantage of this method is the ability to rapidly screen NPs as a DDS. The *in vitro* release model established in these papers cannot represent the complex situation *in vivo*, but, it can provide a convenient way to compare the release profiles between different polymer NPs.

In order to achieve good loading, a polymer NP has to have a well-designed hydrophobic core. For example, in **paper III**, we evaluated different types and shapes of hydrophobic cores and found that the star-like and cholesterol cores are more suitable for drug delivery applications because they have slower release rates. Therefore, the drug release kinetics can be tailored by designing different chemical compositions that control the hydrophobicity of the DDS. However, in **paper I** burst drug release was observed for both DL and HBDL NPs, suggesting that their cores were not sufficiently dense or hydrophobic to keep the drug inside.

One potential way to prevent premature drug release is to covalently link the drug to the polymers.[194] Such linkages eliminate loosely attached drugs and thus avoid rapid drug release.[195] Moreover, introducing chemical bonds that are sensitive to external stimuli might allow the drugs to be released from the NPs only when the stimuli are encountered.[196] pH-responsive linkers are commonly utilized for such purposes.[197] These bonds will break when the NP encounters acidic environments such as endo-lysosomes and the microenvironment of solid tumors, and the NP will then release its cargo.[198,199] In **paper V**, histamine-containing NPs were designed to have pH-responsive drug release. Although no significant differences in drug release were observed between pH 6 and pH 7, NPs with 50% histamine still displayed good properties as a DDS. Considering the good pH responsive behavior seen for a set of similar copolymers,[200] we believe that the pH responsiveness might be hampered by the hydrophobicity of the histamine linker.

Another issue regarding drug encapsulation and release is the need to reduce aggregation after drug loading. Aggregation might occur if DOX is not perfectly loaded into the core. To solve this issue, a proper hydrophilic layer is critical. The most commonly used hydrophilic modification is PEGylation.[45,46,201,202] OEGMA is a good alternative to PEG[203-205] and was utilized in **papers III and IV**. However, hydrophilic shielding alone might not solve the problem completely, and aggregations could still be found for OEGMA-modified NPs in **paper III**. To solve this problem, we introduced negative charges to the system with a cholesterol core and observed a significant reduction in aggregation.

5.2 HYPERBRANCHED POLYMERS *VS.* DENDRIMERS AND DENDRONS

The dendritic polymer family includes dendrimers and dendrons, dendrigrafts, and hyperbranched polymers.[206] Among these, hyperbranched polymers, dendrimers, and dendrons are used in biomedical applications such as drug delivery.[140] But which type is more suitable for use in real medical application in the future?

The bis-MPA-based DL hybrid system was first introduced in the early 1990s by Frechet *et al.*[207] These bis-MPA-based polymers are suitable for biomedical use because of their non-toxic nature and their biodegradable properties.[164,190] In **paper I**, HBDLs were comprehensively compared to their dendron analogs and to DL polymers as a DDS with regard to synthesis, loading capacity, release profile, and efficacy. For the synthesis process, HBDL was produced by a one-step Fisher esterification reaction from the mixture of bis-MPA and PEG monomers. This was much more convenient compared to the synthesis of dendrons from multiple steps,[187] and the HBDLs could be produced on a 50-gram scale. DL micelles expanded less compared to HBDL micelles after encapsulating drugs according to DLS data, and their loading efficiencies were slightly higher implying that DL micelles have better performance regarding drug loading and reducing aggregation after DOX loading. However, this better performance in drug loading did not lead to better release properties. Both DL and HBDL with (pseudo) G3 and G4 cores showed burst release of the drug, and about 80% of the DOX was released within 12 h. HBDL micelles demonstrated slightly slower release than DL micelles. The release rates of these four micelles were much faster compared to bis-MPA dendrimers with a G5 core, which showed less than 40% release after 24 h.[208] This suggests that the hydrophobic cores of current DL or HBDL systems are not sufficient to keep the drug stably encapsulated. In future applications, the hydrophobic core should be expanded. Further comparisons regarding toxicity and efficacy of both systems revealed that they were all non-toxic as pure micelles but demonstrated improved efficacy of loaded DOX. In particular, DOX-HBDLs and DOX-DL with a G4 core displayed 20% greater toxicity to MDA-MB-231 breast cancer cells compared to free DOX. Considering all these aspects, HBDL is a promising alternative to its dendron-based analog because they both have similar properties as a DDS but HBDLs are much easier to produce.

Another consideration in the comparison of hyperbranched polymers vs. dendrimers and dendrons is the intrinsic limitation of micelles formed by amphiphilic copolymers. The micellar structure of an amphiphilic copolymer such as HBDL or DL can only be maintained above the CMC.[209,210] In antitumor applications, micelles are usually administered intravenously and this leads to the dilution of micelles and potential loss of their structural integrity.[79] However, because dendrimers are unimolecular macromolecules they do not have a CMC and are thus considered to be interesting candidates for theranostic platforms.[211,212] Unimolecular micelles can also be produced from hydrophobic dendritic cores that are covalently linked to hydrophilic polymers such as PEG.[136,202,213-215] In **paper IV**, a library of unimolecular micelles was successfully developed from HBDL polymers

that were synthesized from hyperbranched macro-initiators (HBMI) following chain extension using hydrophilic P(OEGMA). P(OEGMA) has been used as a good substitute for PEG.[216,217] These micelles are nontoxic and are capable of encapsulating DOX and delivering it into breast cancer cells with high efficacy. The release profile of these unimolecular micelles was not tailored very well, and this is a common issue for all unimolecular systems, including dendrimers, that use physical drug encapsulation.[218] This can be solved by covalently conjugating drugs to the polymers.[218] In addition, the fluorinated polymer TEFMA was added to the hydrophilic compartments, and this could theoretically provide the micelles with an MRI contrast property and allow them to be used as a theranostic platform. Considering the simple synthesis process compared to dendrimers, hyperbranched unimolecular micelles are indeed a promising approach to developing scalable theranostic systems.

5.3 INTERNALIZATION AND INTRACELLULAR DISTRIBUTION OF POLYMER NPS

5.3.1 Cellular uptake mechanisms of NPs

The primary mechanisms of endocytosis are phagocytosis, macropinocytosis, caveolae-assisted endocytosis, clathrin-mediated endocytosis, as well as clathrin-independent and caveolin-independent endocytosis.[10,142] Phagocytosis is usually found in specialized cells such as macrophages when they eliminate exogenous substances.[142,219] The other mechanisms are commonly investigated regarding cellular uptake of NPs (Figure 4).[220] In **paper II**, a comprehensive investigation into the internalization of bis-MPA-based hyperbranched polymer micelles was performed on the breast cancer cell line MDA-MB-231. The uptake procedure was found to be dependent on time, concentration, and temperature. Further confocal microscope observations and endocytic inhibition assays revealed that NPs were internalized through both macropinocytosis and clathrin-mediated endocytosis rather than caveolae-assisted endocytosis. Particles that are internalized via caveolae-assisted endocytosis are typically around 60 nm,[142,219] which is much smaller than the size of the bis-MPA-based NP used in the paper (average 110 nm), and this explains why caveolae-assisted endocytosis was not a major pathway for these NPs. Clathrin-mediated uptake is the main mechanism of cellular uptake of macromolecules that have a size around 120 nm,[10,140] and this is consistent with our observations. Macropinocytosis is a nonspecific uptake pathway for the internalization of large (>1 μm) and irregularly shaped molecules.[10,220] Although the size of bis-MPA-based hyperbranched NPs in this study (110 nm) was smaller than 1 μm, we still observed the uptake of NPs through this pathway. This might be related to the irregular shape of hyperbranched NPs. Furthermore, intracellular tracking of NPs in early endosomes, lysosomes, and the Golgi network revealed that NPs were mainly found in lysosomes, which is the typical fate of macromolecules internalized via clathrin-mediated endocytosis.[142]

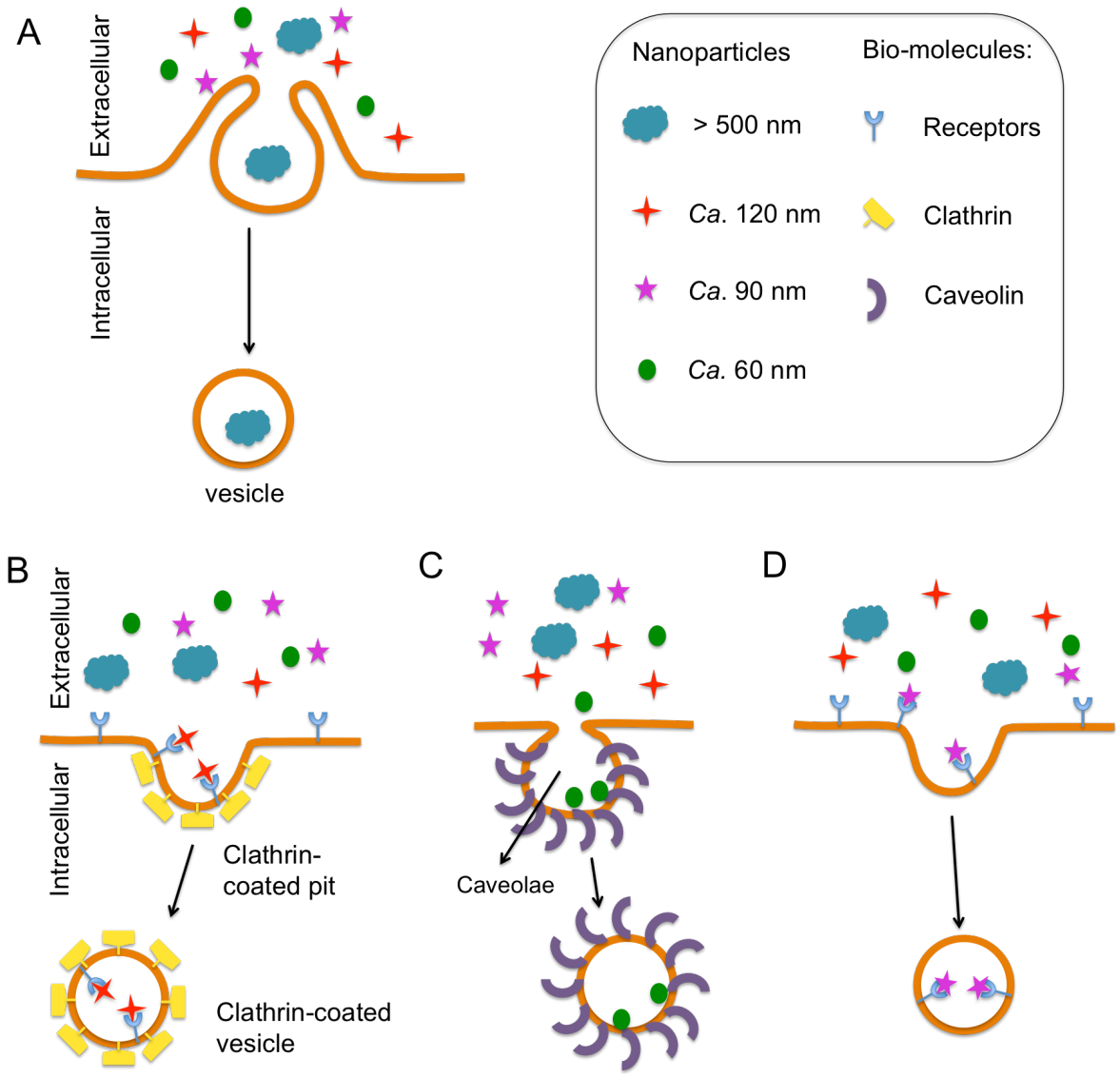

Figure 4. The main mechanisms of cellular uptake of NPs. A) Macropinocytosis, B) clathrin-mediated endocytosis, C) caveolae-mediated endocytosis, D) clathrin-independent and caveolin-independent endocytosis. (The image is modified from DeSimone *et al.*[10])

5.3.2 Endo-lysosomal escape

Polymer-based NPs have been used as DDSs in anticancer research for the last decade, and one important problem that needs to be solved is how to enable NPs to overcome endosomal/lysosomal entrapment so that they can transport their drugs to their targets.[221-224] Endo-lysosomal entrapment is the fate of most exogenous macromolecules, and the acidic environment in endo-lysosomes might lead to the degradation of therapeutic agents.[10,140,220,225,226] One solution to avoiding endo-lysosomal entrapment is to design NPs that can be taken up by caveolae-assisted endocytosis or macropinocytosis.[142] Another option is to design NPs with endo-lysosomal escape properties such as a pH responsive behavior that allows NPs to become positively charged in the acidic environment resulting in the "proton sponge effect" to escape entrapment.[135,221,227,228] In **paper V**, a library of NPs with

functionalized histamine copolymers was produced, and these NPs displayed some ability to escape from endo-lysosomes. This system was developed based on our previous research in which a histamine-functionalized system was reported to show conformation changes in acidic pH due to the positive charges.[200] The capability of endo-lysosomal escape resulting from the introduction of histamine modification was related to the chemical composition of the copolymer. NPs with 50% histamine functionalized in their hydrophobic compartment showed the greatest ability to escape the endo-lysosomes and deliver their drug into the mitochondria and nuclei. Due to its good biocompatibility and pKa in a physiologically relevant pH range (pH 6.0–7.4), histamine has been used to modify other polymer systems for siRNA and drug delivery as reported by Wooley *et al.* and Liu *et al.*, respectively. [229,230]

5.4 THERANOSTIC SYSTEMS – FOCUSING ON MRI DETECTION

As mentioned in the introduction, there are various theranostic systems currently being developed for antitumor applications. Such systems can provide both imaging information about the tumor and therapeutic efficacy during chemotherapeutic therapy.[231,232] Unlike PET, SPECT, and CT, MRI detection does not rely on radioactive agents, and this makes it suitable for theranostic applications that might require multiple administrations. Several systems have been demonstrated for improving MRI contrast, including lipid based,[233] silica based[234,235], and metal based (such as gold NPs[236] and SPION[129]) systems, as well as the fluorinated polymer-based system described in **paper III**. However, silica and lipid-based systems need to introduce gadolinium or other metal-based NPs to serve as contrast agents.[233,234,237] Most metal-based NPs require further coating of lipids or polymers to achieve better biocompatibility and longer blood circulation times.[238,239] In addition, these contrast agents suffer from some disadvantages such as long acquisition time, high background signal from blood and tissue, and toxicity issues caused by the high concentrations of the contrast agents required for ^{1}H-MRI.[84,240,241] On the contrary, fluorinated polymer-based systems do not depend on other magnetic NPs. They can generate a strong ^{19}F signal even though the sensitivity of ^{19}F is 83% that of ^{1}H.[84] Moreover ^{19}F is the only natural isotope of fluorine, and because it is not present in most tissues this leads to low background signals in ^{19}F-MRI.[84] Based on these properties, fluorinated polymers were investigated as potential contrast agents for ^{19}F-MRI.[84,242,243] The NPs that we developed were able to encapsulate drugs, and these could be delivered in a controllable manner by modifying the hydrophobic cores. These same NPs could generate very strong signal for ^{19}F-MRI *in vitro* when they incorporated the fluorine-containing polymer TEFMA. However, our current systems suffer from two limitations. First, because ours is a copolymer system, it has a CMC issue that might limit its application *in vivo*. To solve this issue, we built a library of unimolecular polymers in **paper IV** that do not have a CMC problem. We then added TEFMA to one of these polymer systems and obtained unimolecular micelles with a fluorinated component. Another limitation for the theranostic systems in **paper III** is that they lack targeting molecules, which limits the concentration that can be achieved at the site of the tumor. Therefore, future studies

should add a suitable targeting molecule to try to further improve the accumulation of fluorinated NPs in the tumor area *in vivo*. This approach is based on the work of Thurecht *et al.* who attached folic acid to their fluorinated polymer NPs and achieved ^{19}F-MRI detection of tumors *in vivo*. [244]

5.5 COMPARISON BETWEEN SALIPRO-NPS AND POLYMER-BASED NPS

The salipro-NP described in **paper VI** is a good example of harnessing biomimic properties for nanomedicine applications. Compared to the polymer NPs in this thesis, salipro-lipid NPs demonstrated the highest loading capacity, 95%. The drug encapsulation procedure was very simple, and only entailed incubating hydrophobic lipids and daunorubicin together. Moreover, they showed a slower drug release rate than polymer NPs over a period of 72 h. The slow drug release will enable NPs to better retain their cargo while in circulation and then release it at the tumor site due to EPR effects. However, considering the size of salipro-lipid NPs, which was around 6 nm, further polymer modification might be required for drug delivery applications.

The uptake of salipro-lipid NPs was also very different compared to polymer NPs. Due to their similar composition as the cellular membrane, salipro-lipid NPs tend to fuse with the cell membrane and become trapped there according to the confocal microscopy data. Thus they cannot mediate daunorubicin accumulation in the nuclei as rapidly as histamine-containing NPs, but they can release drugs gradually into the cells and finally achieve distribution in the whole cell. This is consistent with their release profile *in vitro*.

6 CONCLUSIONS

Paper I

- Two novel HBDL and their perfect DL analogues were synthesized using bis-MPA and PEG as building materials.
- One-step Fisher esterification reactions allowed production of HBDL on a larger scale than DL.
- DL showed less aggregation than HBDL after drug loading.
- Both HBDL and DL had burst-like drug release within 12 h indicating the insufficient size of their hydrophobic cores.
- All of the materials were non-toxic to the breast cancer cell line MDA-MB-231, and drug-loaded HBDL tended to have stronger efficacy compared to DL.
- Based on all of the results, we conclude that HBDL can serve as an alterative to DL in biomedical applications, but further refinement is needed for use as a DDS.

Paper II

- A set of bis-MPA-based polymer micelles was synthesized from hyperbranched polyester Boltorn and PEG and labeled with fluorescein.
- bis-MPA-based polymer micelles could be transported into breast cancer cells (MDA-MB-468) via clathrin- and macropinocytosis-mediated endocytosis.
- The uptake process was time, concentration, and energy dependent.

Paper III

- Eight fluorinated polymer NPs with different compositions were synthesized via ATRP.
- The NPs could form by self-assembly of both linear and star-shaped block copolymers.
- These NPs could encapsulate and release DOX, and the drug release kinetics could be tailored by the architecture of the hydrophobic cores.
- All materials were non-toxic to the tested cell lines, but DOX-NPs could induce mitochondrial function loss and significant apoptosis in breast cancer cells
- The *in vitro* MRI measurement demonstrated that the NPs could generate detectable MRI signals.
- Taken together, these results indicate that these fluorinated polymers are promising in theranostic applications.

Paper IV

- Unimolecular micelle NPs were successfully synthesized via a versatile two-step procedure from a library of PEGylated HBDLPs.

- HBDLPs formed predominantly stable and spherical NPs, and the NP dimensions could be tailored by the polymer architecture and hydrophobic/hydrophilic ratio.
- The unimolecular NPs were non-toxic to three breast cancer cell lines (MDA-MB-231, MDA-MB-468, and MCF-7) and one monocyte cell line (RAW 264.7).
- The NPs were able to incorporate and release DOX, and the NPs showed good efficacy against the cancer cells and could be internalized into MDA-MB-468 cells.

Paper V

- A library of histamine-functionalized copolymer micelles was synthesized from PAGE-*b*-PEO via UV-initiated thiol-ene click chemistry.
- The subsequent materials were non-toxic and could self-assemble into polymer micelles to deliver DOX, and they exhibited a higher efficacy in reducing mitochondria function compared to free DOX.
- The histamine modification did not introduce a strong pH-responsive property to the micelles, but the 50% histamine-modified NPs tended to have a slower drug release rate.
- DOX-NPs with 50% and 100% histamine modification exhibited significantly stronger efficacy in 3D models compared to free DOX.
- Histamine-functionalized micelles, in particular the ones with 50% modification in the low molecular weight group, could partly escape from endo-lysosomes and relocate in the mitochondria.

Paper VI

- A stable NP system was successfully developed by enclosing the small human protein saposin A within a hydrophobic lipid core.
- The salipro-NPs could incorporate a variety of lipids, membrane proteins (prokaryotic/eukaryotic), viral antigens, and hydrophobic drugs.
- The salipro-NPs could interact with the cell membrane, and the daunorubicin-encapsulated salipro-NPs could release the drug into breast cancer cells suggesting that such an NP system can be potentially used as a DDS.
- The HIV-1 spike protein (antigen) was also reconstituted into salipro-NPs and maintained in a native and functional state, and this suggests the possibility for the generation of NP-based vaccines for unstable antigens.

7 FUTURE PERSPECTIVES

The studies summarized in this thesis were mainly focused on screening suitable NPs as DDS platforms for breast cancer therapy. These NPs, especially the polymer-based NPs, are theoretically expected to be able to delivery drugs *in vivo* due to the EPR effect, but we have not yet tested any of these systems *in vivo*. For future studies, the following issues should be explored in order to optimize these compounds as a DDS.

We should introduce targeting molecules such as peptides, folic acid, transferrin, antibodies, or aptamers into the polymer systems. This is especially crucial in the case of developing theranostic systems. Our current theranostic systems have shown significant efficacy *in vitro*, but the required concentrations were high at around 10 $mg \cdot mL^{-1}$. Such high concentrations cannot be reached *in vivo* with a single injection; therefore, we need to find a suitable way to achieve active targeting to further increase the local concentration of the NPs at the tumor site.

Furthermore, drugs should be covalently linked to our promising polymer NPs to improve the loading capacity and to introduce a triggered drug release system. Moreover, we should consider dual drug delivery or co-delivery of drugs and siRNA to further improve the therapeutic efficacy via synergistic effects.

With the emergence of novel gene editing tools such as the CRISPR/Cas-9 system, further development of NPs as a delivery system should focus on assisting the somatic delivery of gene editing system to provide better therapies for various diseases.

In addition, the long-term toxicity issue of polymer NPs should be investigated in detail to make sure patients do not suffer additional harm when such constructs progress to clinical testing.

8 ACKNOWLEDGEMENTS

These works were supported by funding from the Swedish Research Council (VR) under grant 2011-3720, and 2009-3259 as well as with support from The Royal Swedish Academy of Sciences, Percy Falks Foundation, Carl Bennet AB, Karolinska Institutet, and VINNOVA - Swedish Governmental Agency for Innovation Systems, and conducted in two divisions of, Karolinska Institutet: Swedish Medical Nanoscience center, Department of Neuroscience and Division of Molecular Toxicology, Institute of Environmental medicine. I would like to express my sincerest gratitude to the people who have supported and helped me:

First of all, I would like to express my deep gratitude to my main supervisor Associate Professor **Andreas Nyström**. I will always remember and thank you for offering me the first chance to work in the scientific field. I will never forget your excellent guidance and supervisions. Deep in my heart, you are not only my supervisor, but also a good friend. I can always get help from you even beside science. I appreciate that a lot!

I also want to thank my co-supervisors, Professor **Bengt Fadeel** and Professor **Agneta Richter-Dahlfors**, for your encouragement, guidance and supports.

Many thanks to my external mentor, Professor **Staffan Svärd**, for your kind advices and support.

Special thanks to **Zeng Xianghui, Zhihua Wu, Maren Diether**, my former group members. It was so nice to work with you guys, and thanks for your contribution in my Ph.D thesis.

I would like to thank all my collaborators, **Christian Porsch, Oliver Andren, Pontus Lundberg, Yvonne Hed, Cosimo Ducani, Åsa Östlund, Peter Damberg, Francisco Vilaplana, Lars Nordstierna, Caroline Janson, Nathaniel Lynd, Jens Frauenfeld, Robin Löving, Lin Zhu, Caroline Jegerschöld, Fatma Guettou, Per Moberg, Christian Löw, Henrik Garoff, Pär Nordlund, Michael Malkoch, Eva Malmström, Craig Hawker.** I appreciate your contributions and hope to collaborate with you again in future!

Warm thanks to my colleague and friends in Swedish Nanoscience Center: **Alan, Cosimo, Erik, Björn, Xianken, Sten Friberg, Susanne, Klas, Margret, Peter, Karl, Jorrit, Karin.**

Great thanks to my present and former colleagues from IMM: **Hanna, Anda, Sebastiano, Lucian, Audrey, Teresa, Kunal, Sourav, Malahat, Breatrice, Katharina, Fernando, Akihiro, Olesja, Ramy, Neus,** Thank you for the nice environment, discussion, fika and parties. These are precious memories in my life!

I would also like to thank my Chinese friends who made my life in Sweden happy and easy. Thanks to **Kai Du & Qin Xiao, Jianren Song & Na Guan, Huan Song & Jianwei Zhu, Xinming Wang & Yang Xu, Xiaoyuan Ren & Rong Jiang, Zheng Chang & Ci Song, Qi Jia, Qiang Ma, Qiang Zhang, Yixin Wang, Dong Yang, Chen Suo, Tianwei Gu, Yang Xuan, Lidi Xu, Qiongzi, Hao Yu.** I will always remember the wonderful time spend with

you guys. Special thanks to **Zhe Jin & Qiaolin Deng**, for all your kindly suggestion and help!

I also want to thank some family friends, **Yan Wang, Emily & Tor.**

Finally, I would like to thank my family and all my relatives. Thanks to my **parents** who always support me 100% for my each decision, I will never let you down. Especially to my dear **Menghan**, my lovely wife, I am very lucky to have you around me. There are no words that can be competent to express my gratitude to you, so I just want to say: I love you!

9 REFERENCES

1 Weigelt, B., Peterse, J. L. & van 't Veer, L. J. Breast cancer metastasis: markers and models. *Nat Rev Cancer* **5**, 591-602, doi:10.1038/nrc1670 (2005).

2 Duncan, R. Polymer conjugates as anticancer nanomedicines. *Nat Rev Cancer* **6**, 688-701, doi:Doi 10.1038/Nrc1958 (2006).

3 Ferrari, M. Cancer nanotechnology: Opportunities and challenges. *Nat Rev Cancer* **5**, 161-171, doi:Doi 10.1038/Nrc1566 (2005).

4 Yezhelyev, M. V. *et al.* Emerging use of nanoparticles in diagnosis and treatment of breast cancer. *Lancet Oncol* **7**, 657-667, doi:Doi 10.1016/S1470-2045(06)70793-8 (2006).

5 Altinoglu, E. I. *et al.* Near-infrared emitting fluorophore-doped calcium phosphate nanoparticles for in vivo imaging of human breast cancer. *Acs Nano* **2**, 2075-2084, doi:10.1021/nn800448r (2008).

6 Yang, L. *et al.* Receptor-targeted nanoparticles for in vivo imaging of breast cancer. *Clin Cancer Res* **15**, 4722-4732, doi:10.1158/1078-0432.CCR-08-3289 (2009).

7 Zunino, F., Dimarco, A., Zaccara, A. & Gambetta, R. A. The Interaction of Daunorubicin and Doxorubicin with DNA and Chromatin. *Biochim Biophys Acta* **607**, 206-214, doi:Doi 10.1016/0005-2787(80)90073-8 (1980).

8 Singal, P. K. & Iliskovic, N. Doxorubicin-induced cardiomyopathy. *New Engl J Med* **339**, 900-905, doi:Doi 10.1056/Nejm199809243391307 (1998).

9 Barenholz, Y. Doxil (R) - The first FDA-approved nano-drug: Lessons learned. *J Control Release* **160**, 117-134, doi:Doi 10.1016/J.Jconrel.2012.03.020 (2012).

10 Petros, R. A. & DeSimone, J. M. Strategies in the design of nanoparticles for therapeutic applications. *Nat Rev Drug Discov* **9**, 615-627, doi:Doi 10.1038/Nrd2591 (2010).

11 Tang, S. *et al.* Co-delivery of doxorubicin and RNA using pH-sensitive poly (beta-amino ester) nanoparticles for reversal of multidrug resistance of breast cancer. *Biomaterials* **35**, 6047-6059, doi:Doi 10.1016/J.Biomaterials.2014.04.025 (2014).

12 Cai, D. F. *et al.* Hydrophobic penetrating peptide PFVYLI-modified stealth liposomes for doxorubicin delivery in breast cancer therapy. *Biomaterials* **35**, 2283-2294, doi:Doi 10.1016/J.Biomaterials.2013.11.088 (2014).

13 Yang, Y., Pan, D. Y., Luo, K., Li, L. & Gu, Z. W. Biodegradable and amphiphilic block copolymer-doxorubicin conjugate as polymeric nanoscale drug delivery vehicle for breast cancer therapy. *Biomaterials* **34**, 8430-8443, doi:Doi 10.1016/J.Biomaterials.2013.07.037 (2013).

14 Wang, L. *et al.* Fluorescence resonant energy transfer biosensor based on upconversion-luminescent nanoparticles. *Angewandte Chemie* **44**, 6054-6057, doi:10.1002/anie.200501907 (2005).

15 Jia, J. *et al.* A method to construct a third-generation horseradish peroxidase biosensor: self-assembling gold nanoparticles to three-dimensional sol-gel network. *Anal Chem* **74**, 2217-2223 (2002).

16 Hrapovic, S., Liu, Y. L., Male, K. B. & Luong, J. H. T. Electrochemical biosensing platforms using platinum nanoparticles and carbon nanotubes. *Anal Chem* **76**, 1083-1088, doi:Doi 10.1021/Ac035143t (2004).

17 Harrison, B. S. & Atala, A. Carbon nanotube applications for tissue engineering. *Biomaterials* **28**, 344-353, doi:10.1016/j.biomaterials.2006.07.044 (2007).

18 Shi, J., Votruba, A. R., Farokhzad, O. C. & Langer, R. Nanotechnology in drug delivery and tissue engineering: from discovery to applications. *Nano Lett* **10**, 3223-3230, doi:10.1021/nl102184c (2010).

19 Goldberg, M., Langer, R. & Jia, X. Nanostructured materials for applications in drug delivery and tissue engineering. *Journal of biomaterials science. Polymer edition* **18**, 241-268 (2007).

20 Erathodiyil, N. & Ying, J. Y. Functionalization of Inorganic Nanoparticles for Bioimaging Applications. *Accounts Chem Res* **44**, 925-935, doi:Doi 10.1021/Ar2000327 (2011).

21 Frey, N. A., Peng, S., Cheng, K. & Sun, S. H. Magnetic nanoparticles: synthesis, functionalization, and applications in bioimaging and magnetic energy storage. *Chem Soc Rev* **38**, 2532-2542, doi:Doi 10.1039/B815548h (2009).

22 Sharma, P., Brown, S., Walter, G., Santra, S. & Moudgil, B. Nanoparticles for bioimaging. *Advances in colloid and interface science* **123-126**, 471-485, doi:10.1016/j.cis.2006.05.026 (2006).

23 Brigger, I., Dubernet, C. & Couvreur, P. Nanoparticles in cancer therapy and diagnosis. *Adv Drug Deliver Rev* **64**, 24-36, doi:Doi 10.1016/J.Addr.2012.09.006 (2012).

24 Georganopoulou, D. G. *et al.* Nanoparticle-based detection in cerebral spinal fluid of a soluble pathogenic biomarker for Alzheimer's disease. *Proceedings of the National Academy of Sciences of the United States of America* **102**, 2273-2276, doi:Doi 10.1073/Pnas.0409336102 (2005).

25 Wang, Y. F. *et al.* Visual gene diagnosis of HBV and HCV based on nanoparticle probe amplification and silver staining enhancement. *J Med Virol* **70**, 205-211, doi:Doi 10.1002/Jmv.10379 (2003).

26 Mornet, S., Vasseur, S., Grasset, F. & Duguet, E. Magnetic nanoparticle design for medical diagnosis and therapy. *J Mater Chem* **14**, 2161-2175, doi:Doi 10.1039/B402025a (2004).

27 Pornpattananangkul, D. *et al.* Bacterial Toxin-Triggered Drug Release from Gold Nanoparticle-Stabilized Liposomes for the Treatment of Bacterial Infection. *J Am Chem Soc* **133**, 4132-4139, doi:Doi 10.1021/Ja111110e (2011).

28 Roney, C. *et al.* Targeted nanoparticles for drug delivery through the blood-brain barrier for Alzheimer's disease. *J Control Release* **108**, 193-214, doi:Doi 10.1016/J.Jconrel.2005.07.024 (2005).

29 Brannon-Peppas, L. & Blanchette, J. O. Nanoparticle and targeted systems for cancer therapy. *Adv Drug Deliver Rev* **64**, 206-212, doi:Doi 10.1016/J.Addr.2012.09.033 (2012).

30 Hrkach, J. *et al.* Preclinical development and clinical translation of a PSMA-targeted docetaxel nanoparticle with a differentiated pharmacological profile. *Science translational medicine* **4**, 128ra139, doi:10.1126/scitranslmed.3003651 (2012).

31 Davis, M. E. *et al.* Evidence of RNAi in humans from systemically administered siRNA via targeted nanoparticles. *Nature* **464**, 1067-1070, doi:10.1038/nature08956 (2010).

32 Feldman, E. J. *et al.* First-In-Man Study of CPX-351: A Liposomal Carrier Containing Cytarabine and Daunorubicin in a Fixed 5:1 Molar Ratio for the Treatment of Relapsed and Refractory Acute Myeloid Leukemia. *J Clin Oncol* **29**, 979-985, doi:Doi 10.1200/Jco.2010.30.5961 (2011).

33 Pittet, L. *et al.* Development and preclinical evaluation of SEL-068, a novel targeted Synthetic Vaccine Particle (tSVP (TM)) for smoking cessation and relapse prevention that generates high titers of antibodies against nicotine. *J Immunol* **188** (2012).

34 Valle, J. W. *et al.* A phase 2 study of SP1049C, doxorubicin in P-glycoprotein-targeting pluronics, in patients with advanced adenocarcinoma of the esophagus and gastroesophageal junction. *Invest New Drug* **29**, 1029-1037, doi:Doi 10.1007/S10637-010-9399-1 (2011).

35 Roby, K. F. *et al.* Syngeneic mouse model of epithelial ovarian cancer: Effects of nanoparticulate paclitaxel, Nanotax (R). *Adv Exp Med Biol* **622**, 169-181 (2008).

36 Gaillard, P. J. *et al.* Pharmacokinetics, Brain Delivery, and Efficacy in Brain Tumor-Bearing Mice of Glutathione Pegylated Liposomal Doxorubicin (2B3-101). *Plos One* **9**, doi:ARTN e82331, DOI 10.1371/journal.pone.0082331 (2014).

37 Scheffel, U., Rhodes, B. A., Natarajan, T. K. & Wagner, H. N., Jr. Albumin microspheres for study of the reticuloendothelial system. *Journal of nuclear medicine : official publication, Society of Nuclear Medicine* **13**, 498-503 (1972).

38 Matsumura, Y. & Maeda, H. A New Concept for Macromolecular Therapeutics in Cancer-Chemotherapy - Mechanism of Tumoritropic Accumulation of Proteins and the Antitumor Agent Smancs. *Cancer Res* **46**, 6387-6392 (1986).

39 Maeda, H., Greish, K. & Fang, J. The EPR effect and polymeric drugs: A paradigm shift for cancer chemotherapy in the 21st century. *Adv Polym Sci* **193**, 103-121, doi:Doi 10.1007/12_026 (2006).

40 Vivero-Escoto, J. L., Slowing, I. I., Wu, C. W. & Lin, V. S. Y. Photoinduced Intracellular Controlled Release Drug Delivery in Human Cells by Gold-Capped Mesoporous Silica Nanosphere. *J Am Chem Soc* **131**, 3462-+, doi:Doi 10.1021/Ja900025f (2009).

41 zur Muhlen, A., Schwarz, C. & Mehnert, W. Solid lipid nanoparticles (SLN) for controlled drug delivery - Drug release and release mechanism. *Eur J Pharm Biopharm* **45**, 149-155, doi:Doi 10.1016/S0939-6411(97)00150-1 (1998).

42 Mu, L. & Feng, S. S. A novel controlled release formulation for the anticancer drug paclitaxel (Taxol (R)): PLGA nanoparticles containing vitamin E TPGS. *J Control Release* **86**, 33-48, doi:Pii S0168-3659(02)00320-6, Doi 10.1016/S0168-3659(02)00320-6 (2003).

43 Slowing, I. I., Vivero-Escoto, J. L., Wu, C. W. & Lin, V. S. Y. Mesoporous silica nanoparticles as controlled release drug delivery and gene transfection carriers. *Adv Drug Deliver Rev* **60**, 1278-1288, doi:Doi 10.1016/J.Addr.2008.03.012 (2008).

44 Elzoghby, A. O., Samy, W. M. & Elgindy, N. A. Albumin-based nanoparticles as potential controlled release drug delivery systems. *J Control Release* **157**, 168-182, doi:Doi 10.1016/J.Jconrel.2011.07.031 (2012).

45 Otsuka, H., Nagasaki, Y. & Kataoka, K. PEGylated nanoparticles for biological and pharmaceutical applications. *Adv Drug Deliver Rev* **64**, 246-255, doi:Doi 10.1016/J.Addr.2012.09.022 (2012).

46 Peracchia, M. T. *et al.* Stealth PEGylated polycyanoacrylate nanoparticles for intravenous administration and splenic targeting. *J Control Release* **60**, 121-128 (1999).

47 Mitra, S., Gaur, U., Ghosh, P. C. & Maitra, A. N. Tumour targeted delivery of encapsulated dextran-doxorubicin conjugate using chitosan nanoparticles as carrier. *J Control Release* **74**, 317-323, doi:Doi 10.1016/S0168-3659(01)00342-X (2001).

48 Farokhzad, O. C. *et al.* Nanoparticle-aptamer bioconjugates: a new approach for targeting prostate cancer cells. *Cancer Res* **64**, 7668-7672, doi:10.1158/0008-5472.CAN-04-2550 (2004).

49 Davis, M. E. The first targeted delivery of siRNA in humans via a self-assembling, cyclodextrin polymer-based nanoparticle: from concept to clinic. *Molecular pharmaceutics* **6**, 659-668, doi:10.1021/mp900015y (2009).

50 Medarova, Z., Pham, W., Farrar, C., Petkova, V. & Moore, A. In vivo imaging of siRNA delivery and silencing in tumors. *Nat Med* **13**, 372-377, doi:Doi 10.1038/Nm1486 (2007).

51 Lee, H. *et al.* Molecularly self-assembled nucleic acid nanoparticles for targeted in vivo siRNA delivery. *Nat Nanotechnol* **7**, 389-393, doi:Doi 10.1038/Nnano.2012.73 (2012).

52 Roy, K., Mao, H. Q., Huang, S. K. & Leong, K. W. Oral gene delivery with chitosan-DNA nanoparticles generates immunologic protection in a murine model of peanut allergy. *Nat Med* **5**, 387-391 (1999).

53 Mao, H. Q. *et al.* Chitosan-DNA nanoparticles as gene carriers: synthesis, characterization and transfection efficiency. *J Control Release* **70**, 399-421, doi:Doi 10.1016/S0168-3659(00)00361-8 (2001).

54 Smith, D. M., Simon, J. K. & Baker, J. R. Applications of nanotechnology for immunology. *Nat Rev Immunol* **13**, 592-605, doi:Doi 10.1038/Nri3488 (2013).

55 Veiseh, O., Tang, B. C., Whitehead, K. A., Anderson, D. G. & Langer, R. Managing diabetes with nanomedicine: challenges and opportunities. *Nat Rev Drug Discov* **14**, 45-57, doi:Doi 10.1038/Nrd4477 (2015).

56 Jain, R. K. & Stylianopoulos, T. Delivering nanomedicine to solid tumors. *Nat Rev Clin Oncol* **7**, 653-664, doi:Doi 10.1038/Nrclinonc.2010.139 (2010).

57 Srikanth, M. & Kessler, J. A. Nanotechnology-novel therapeutics for CNS disorders. *Nat Rev Neurol* **8**, 307-318, doi:Doi 10.1038/Nrneurol.2012.76 (2012).

58 Contreras-Ruiz, L. *et al.* A nanomedicine to treat ocular surface inflammation: performance on an experimental dry eye murine model. *Gene Ther* **20**, 467-477, doi:Doi 10.1038/Gt.2012.56 (2013).

59 Konno, T., Watanabe, J. & Ishihara, K. Enhanced solubility of paclitaxel using water-soluble and biocompatible 2-methacryloyloxyethyl phosphorylcholine polymers. *J Biomed Mater Res A* **65A**, 209-214, doi:Doi 10.1002/Jbm.A.10481 (2003).

60 Park, E. K., Kim, S. Y., Lee, S. B. & Lee, Y. M. Folate-conjugated methoxy poly(ethylene glycol)/poly(epsilon-caprolactone) amphiphilic block copolymeric micelles for tumor-targeted drug delivery. *J Control Release* **109**, 158-168, doi:Doi 10.1016/J.Jconrel.2005.09.039 (2005).

61 Gabizon, A. *et al.* Prolonged Circulation Time and Enhanced Accumulation in Malignant Exudates of Doxorubicin Encapsulated in Polyethylene-Glycol Coated Liposomes. *Cancer Res* **54**, 987-992 (1994).

62 Prencipe, G. *et al.* PEG Branched Polymer for Functionalization of Nanomaterials with Ultralong Blood Circulation. *J Am Chem Soc* **131**, 4783-4787, doi:Doi 10.1021/Ja809086q (2009).

63 Gref, R. *et al.* 'Stealth' corona-core nanoparticles surface modified by polyethylene glycol (PEG): influences of the corona (PEG chain length and surface density) and of the core composition on phagocytic uptake and plasma protein adsorption. *Colloid Surface B* **18**, 301-313, doi:Doi 10.1016/S0927-7765(99)00156-3 (2000).

64 Li, S. D. & Huang, L. Nanoparticles evading the reticuloendothelial system: Role of the supported bilayer. *Bba-Biomembranes* **1788**, 2259-2266, doi:Doi 10.1016/J.Bbamem.2009.06.022 (2009).

65 Wissing, S. A., Kayser, O. & Muller, R. H. Solid lipid nanoparticles for parenteral drug delivery. *Adv Drug Deliver Rev* **56**, 1257-1272, doi:Doi 10.1016/J.Addr.2003.12.002 (2004).

66 Liu, Z. H., Jiao, Y. P., Wang, Y. F., Zhou, C. R. & Zhang, Z. Y. Polysaccharides-based nanoparticles as drug delivery systems. *Adv Drug Deliver Rev* **60**, 1650-1662, doi:Doi 10.1016/J.Addr.2008.09.001 (2008).

67 O'Brien, M. E. *et al.* Reduced cardiotoxicity and comparable efficacy in a phase III trial of pegylated liposomal doxorubicin HCl (CAELYX/Doxil) versus conventional doxorubicin for first-line treatment of metastatic breast cancer. *Annals of oncology : official journal of the European Society for Medical Oncology / ESMO* **15**, 440-449 (2004).

68 Safra, T. *et al.* Pegylated liposomal doxorubicin (doxil): reduced clinical cardiotoxicity in patients reaching or exceeding cumulative doses of 500 mg/m2. *Annals of oncology : official journal of the European Society for Medical Oncology / ESMO* **11**, 1029-1033 (2000).

69 Yin, H. *et al.* Non-viral vectors for gene-based therapy. *Nat Rev Genet* **15**, 541-555, doi:Doi 10.1038/Nrg3763 (2014).

70 Mao, S. R., Sun, W. & Kissel, T. Chitosan-based formulations for delivery of DNA and siRNA. *Adv Drug Deliver Rev* **62**, 12-27, doi:Doi 10.1016/J.Addr.2009.08.004 (2010).

71 Xia, T. A. *et al.* Polyethyleneimine Coating Enhances the Cellular Uptake of Mesoporous Silica Nanoparticles and Allows Safe Delivery of siRNA and DNA Constructs. *Acs Nano* **3**, 3273-3286, doi:Doi 10.1021/Nn900918w (2009).

72 Byrne, J. D., Betancourt, T. & Brannon-Peppas, L. Active targeting schemes for nanoparticle systems in cancer therapeutics. *Adv Drug Deliver Rev* **60**, 1615-1626, doi:Doi 10.1016/J.Addr.2008.08.005 (2008).

73 Cho, K. J., Wang, X., Nie, S. M., Chen, Z. & Shin, D. M. Therapeutic nanoparticles for drug delivery in cancer. *Clin Cancer Res* **14**, 1310-1316, doi:Doi 10.1158/1078-0432.Ccr-07-1441 (2008).

74 Davis, M. E., Chen, Z. & Shin, D. M. Nanoparticle therapeutics: an emerging treatment modality for cancer. *Nat Rev Drug Discov* **7**, 771-782, doi:Doi 10.1038/Nrd2614 (2008).

75 Nasongkla, N. *et al.* Multifunctional polymeric micelles as cancer-targeted, MRI-ultrasensitive drug delivery systems. *Nano Lett* **6**, 2427-2430, doi:Doi 10.1021/Nl061412u (2006).

76 Gao, J. H., Gu, H. W. & Xu, B. Multifunctional Magnetic Nanoparticles: Design, Synthesis, and Biomedical Applications. *Accounts Chem Res* **42**, 1097-1107, doi:Doi 10.1021/Ar9000026 (2009).

77 Turner, J. L. *et al.* Synthesis of gadolinium-labeled shell-crosslinked nanoparticles for magnetic resonance imaging applications. *Adv Funct Mater* **15**, 1248-1254, doi:Doi 10.1002/Adfm.200500005 (2005).

78 Talelli, M. *et al.* Superparamagnetic iron oxide nanoparticles encapsulated in biodegradable thermosensitive polymeric micelles: toward a targeted nanomedicine suitable for image-guided drug delivery. *Langmuir : the ACS journal of surfaces and colloids* **25**, 2060-2067, doi:10.1021/la8036499 (2009).

79 Guo, J. *et al.* Image-guided and tumor-targeted drug delivery with radiolabeled unimolecular micelles. *Biomaterials* **34**, 8323-8332, doi:10.1016/j.biomaterials.2013.07.085 (2013).

80 Simone, E. A. *et al.* Endothelial targeting of polymeric nanoparticles stably labeled with the PET imaging radioisotope iodine-124. *Biomaterials* **33**, 5406-5413, doi:10.1016/j.biomaterials.2012.04.036 (2012).

81 Polyak, A. *et al.* In vitro and biodistribution examinations of Tc-99m-labelled doxorubicin-loaded nanoparticles. *Nuclear medicine review. Central & Eastern Europe* **14**, 55-62 (2011).

82 Antoch, G. *et al.* Comparison of PET, CT, and dual-modality PET/CT imaging for monitoring of imatinib (STI571) therapy in patients with gastrointestinal stromal tumors. *Journal of Nuclear Medicine* **45**, 357-365 (2004).

83 Nystrom, A. M. & Wooley, K. L. The importance of Chemistry in Creating Well-Defined Nanoscopic Embedded Therapeutics: Devices Capable of the Dual Functions of Imaging and Therapy. *Accounts Chem Res* **44**, 969-978, doi:Doi 10.1021/Ar200097k (2011).

84 Tirotta, I. *et al.* (19)F magnetic resonance imaging (MRI): from design of materials to clinical applications. *Chem Rev* **115**, 1106-1129, doi:10.1021/cr500286d (2015).

85 Gupta, A. K. & Wells, S. Surface-modified superparamagnetic nanoparticles for drug delivery: Preparation, characterization, and cytotoxicity studies. *Ieee T Nanobiosci* **3**, 66-73, doi:Doi 10.1109/Tnb.2003.820277 (2004).

86 Han, H. D. *et al.* Targeted Gene Silencing Using RGD-Labeled Chitosan Nanoparticles. *Clin Cancer Res* **16**, 3910-3922, doi:Doi 10.1158/1078-0432.Ccr-10-0005 (2010).

87 Danhier, F. *et al.* Targeting of tumor endothelium by RGD-grafted PLGA-nanoparticles loaded with Paclitaxel. *J Control Release* **140**, 166-173, doi:Doi 10.1016/J.Jconrel.2009.08.011 (2009).

88 Lee, H. Y. *et al.* PET/MRI dual-modality tumor imaging using arginine-glycine-aspartic (RGD) - Conjugated radiolabeled iron oxide nanoparticles. *Journal of Nuclear Medicine* **49**, 1371-1379, doi:Doi 10.2967/Jnumed.108.051243 (2008).

89 Liu, L. H. *et al.* Self-assembled cationic peptide nanoparticles as an efficient antimicrobial agent. *Nat Nanotechnol* **4**, 457-463, doi:Doi 10.1038/Nnano.2009.153 (2009).

90 Lipka, J. *et al.* Biodistribution of PEG-modified gold nanoparticles following intratracheal instillation and intravenous injection. *Biomaterials* **31**, 6574-6581, doi:10.1016/j.biomaterials.2010.05.009 (2010).

91 Yang, W., Peters, J. I. & Williams, R. O. Inhaled nanoparticles - A current review. *Int J Pharmaceut* **356**, 239-247, doi:Doi 10.1016/J.Ijpharm.2008.02.011 (2008).

92 Yang, S. C. *et al.* Body distribution in mice of intravenously injected camptothecin solid lipid nanoparticles and targeting effect on brain. *J Control Release* **59**, 299-307, doi:Doi 10.1016/S0168-3659(99)00007-3 (1999).

93 Mutlu, G. M. *et al.* Biocompatible Nanoscale Dispersion of Single-Walled Carbon Nanotubes Minimizes in vivo Pulmonary Toxicity. *Nano Lett* **10**, 1664-1670, doi:Doi 10.1021/Nl9042483 (2010).

94 Sonaje, K. *et al.* In vivo evaluation of safety and efficacy of self-assembled nanoparticles for oral insulin delivery. *Biomaterials* **30**, 2329-2339, doi:Doi 10.1016/J.Biomaterials.2008.12.066 (2009).

95 Powell, J. J., Faria, N., Thomas-McKay, E. & Pele, L. C. Origin and fate of dietary nanoparticles and microparticles in the gastrointestinal tract. *J Autoimmun* **34**, J226-J233, doi:Doi 10.1016/J.Jaut.2009.11.006 (2010).

96 Cheng, C. J., Tietjen, G. T., Saucier-Sawyer, J. K. & Saltzman, W. M. A holistic approach to targeting disease with polymeric nanoparticles. *Nat Rev Drug Discov*, doi:10.1038/nrd4503 (2015).

97 Vinogradov, S. V., Bronich, T. K. & Kabanov, A. V. Nanosized cationic hydrogels for drug delivery: preparation, properties and interactions with cells. *Adv Drug Deliver Rev* **54**, 135-147, doi:Doi 10.1016/S0169-409x(01)00245-9 (2002).

98 Parrott, M. C. *et al.* Synthesis, Radiolabeling, and Bio-imaging of High-Generation Polyester Dendrimers. *J Am Chem Soc* **131**, 2906-2916, doi:Doi 10.1021/Ja8078175 (2009).

99 Koo, H. *et al.* In Vivo Targeted Delivery of Nanoparticles for Theranosis. *Accounts Chem Res* **44**, 1018-1028, doi:Doi 10.1021/Ar2000138 (2011).

100 Yang, Q. *et al.* Evading Immune Cell Uptake and Clearance Requires PEG Grafting at Densities Substantially Exceeding the Minimum for Brush Conformation. *Molecular pharmaceutics* **11**, 1250-1258, doi:Doi 10.1021/Mp400703d (2014).

101 Ishihara, T. *et al.* Evasion of the Accelerated Blood Clearance Phenomenon by Coating of Nanoparticles with Various Hydrophilic Polymers. *Biomacromolecules* **11**, 2700-2706, doi:Doi 10.1021/Bm100754e (2010).

102 Storm, G., Belliot, S. O., Daemen, T. & Lasic, D. D. Surface Modification of Nanoparticles to Oppose Uptake by the Mononuclear Phagocyte System. *Adv Drug Deliver Rev* **17**, 31-48, doi:Doi 10.1016/0169-409x(95)00039-A (1995).

103 Dobrovolskaia, M. A., Aggarwal, P., Hall, J. B. & McNeil, S. E. Preclinical studies to understand nanoparticle interaction with the immune system and its potential effects on nanoparticle biodistribution. *Molecular pharmaceutics* **5**, 487-495, doi:Doi 10.1021/Mp800032f (2008).

104 Szebeni, J. Complement activation-related pseudoallergy: A stress reaction in blood triggered by nanomedicines and biologicals. *Mol Immunol* **61**, 163-173, doi:Doi 10.1016/J.Molimm.2014.06.038 (2014).

105 Hamad, I. *et al.* Complement activation by PEGylated single-walled carbon nanotubes is independent of C1q and alternative pathway turnover. *Mol Immunol* **45**, 3797-3803, doi:Doi 10.1016/J.Molimm.2008.05.020 (2008).

106 Hamad, I., Hunter, A. C., Szebeni, J. & Moghimi, S. M. Poly(ethylene glycol)s generate complement activation products in human serum through increased alternative pathway turnover and a MASP-2-dependent process. *Mol Immunol* **46**, 225-232, doi:10.1016/j.molimm.2008.08.276 (2008).

107 Garay, R. P., El-Gewely, R., Armstrong, J. K., Garratty, G. & Richette, P. Antibodies against polyethylene glycol in healthy subjects and in patients treated with PEG-conjugated agents. *Expert Opin Drug Del* **9**, 1319-1323, doi:Doi 10.1517/17425247.2012.720969 (2012).

108 van den Hoven, J. M. *et al.* Complement activation by PEGylated liposomes containing prednisolone. *Eur J Pharm Sci* **49**, 265-271, doi:Doi 10.1016/J.Ejps.2013.03.007 (2013).

109 Hamad, I. *et al.* Distinct Polymer Architecture Mediates Switching of Complement Activation Pathways at the Nanosphere-Serum Interface: Implications for Stealth Nanoparticle Engineering. *Acs Nano* **4**, 6629-6638, doi:Doi 10.1021/Nn101990a (2010).

110 Janos, S. & Moghimi, S. M. Liposome triggering of innate immune responses: A perspective on benefits and adverse reactions. *J Liposome Res* **19**, 85-90, doi:Doi 10.1080/08982100902792855 (2009).

111 Moghimi, S. M. & Szebeni, J. Stealth liposomes and long circulating nanoparticles: critical issues in pharmacokinetics, opsonization and protein-binding properties. *Prog Lipid Res* **42**, 463-478, doi:Doi 10.1016/S0163-7827(03)00033-X (2003).

112 Torchilin, V. Tumor delivery of macromolecular drugs based on the EPR effect. *Adv Drug Deliver Rev* **63**, 131-135, doi:Doi 10.1016/J.Addr.2010.03.011 (2011).

113 Bardhan, R., Lal, S., Joshi, A. & Halas, N. J. Theranostic Nanoshells: From Probe Design to Imaging and Treatment of Cancer. *Accounts Chem Res* **44**, 936-946, doi:Doi 10.1021/Ar200023x (2011).

114 Shi, J. J., Xiao, Z. Y., Kamaly, N. & Farokhzad, O. C. Self-Assembled Targeted Nanoparticles: Evolution of Technologies and Bench to Bedside Translation. *Accounts Chem Res* **44**, 1123-1134, doi:Doi 10.1021/Ar200054n (2011).

115 Stella, B. *et al.* Design of folic acid-conjugated nanoparticles for drug targeting. *J Pharm Sci* **89**, 1452-1464, doi:Doi 10.1002/1520-6017(200011)89:11<1452::Aid-Jps8>3.0.Co;2-P (2000).

116 Davis, M. E. The First Targeted Delivery of siRNA in Humans via a Self-Assembling, Cyclodextrin Polymer-Based Nanoparticle: From Concept to Clinic. *Molecular pharmaceutics* **6**, 659-668, doi:Doi 10.1021/Mp900015y (2009).

117 Kocbek, P., Obermajer, N., Cegnar, M., Kos, J. & Kristl, J. Targeting cancer cells using PLGA nanoparticles surface modified with monoclonal antibody. *J Control Release* **120**, 18-26, doi:Doi 10.1016/J.Jconrel.2007.03.012 (2007).

118 van der Meel, R., Vehmeijer, L. J. C., Kok, R. J., Storm, G. & van Gaal, E. V. B. Ligand-targeted particulate nanomedicines undergoing clinical evaluation: Current status. *Adv Drug Deliver Rev* **65**, 1284-1298, doi:Doi 10.1016/J.Addr.2013.08.012 (2013).

119 Xu, L. *et al.* Systemic tumor-targeted gene delivery by anti-transferrin receptor scFv-immunoliposomes. *Mol Cancer Ther* **1**, 337-346 (2002).

120 Xu, L. *et al.* Systemic p53 gene therapy of cancer with immunolipoplexes targeted by anti-transferrin receptor scFv. *Mol Med* **7**, 723-734 (2001).

121 Suzuki, R. *et al.* Effective anti-tumor activity of oxaliplatin encapsulated in transferrin-PEG-liposome. *Int J Pharmaceut* **346**, 143-150, doi:Doi 10.1016/J.Ijpharm.2007.06.010 (2008).

122 Salvati, A. *et al.* Transferrin-functionalized nanoparticles lose their targeting capabilities when a biomolecule corona adsorbs on the surface. *Nat Nanotechnol* **8**, 137-143, doi:Doi 10.1038/Nnano.2012.237 (2013).

123 Kirpotin, D. B. *et al.* Antibody targeting of long-circulating lipidic nanoparticles does not increase tumor localization but does increase internalization in animal models. *Cancer Res* **66**, 6732-6740, doi:Doi 10.1158/0008-5472.Can-05-4199 (2006).

124 Bartlett, D. W., Su, H., Hildebrandt, I. J., Weber, W. A. & Davis, M. E. Impact of tumor-specific targeting on the biodistribution and efficacy of siRNA nanoparticles measured by multimodality in vivo imaging. *Proceedings of the National Academy of Sciences of the United States of America* **104**, 15549-15554, doi:Doi 10.1073/Pnas.0707461104 (2007).

125 Parker, N. *et al.* Folate receptor expression in carcinomas and normal tissues determined by a quantitative radioligand binding assay. *Anal Biochem* **338**, 284-293, doi:Doi 10.1016/J.Ab.2004.12.026 (2005).

126 Kawabata, H. *et al.* Expression of transferrin receptor 2 in normal and neoplastic hematopoietic cells. *Blood* **98**, 2714-2719, doi:Doi 10.1182/Blood.V98.9.2714 (2001).

127 Oh, J. K. & Park, J. M. Iron oxide-based superparamagnetic polymeric nanomaterials: Design, preparation, and biomedical application. *Prog Polym Sci* **36**, 168-189, doi:Doi 10.1016/J.Progpolymsci.2010.08.005 (2011).

128 Popovtzer, R. *et al.* Targeted Gold Nanoparticles Enable Molecular CT Imaging of Cancer. *Nano Lett* **8**, 4593-4596, doi:Doi 10.1021/Nl8029114 (2008).

129 Cabral, H., Nishiyama, N. & Kataoka, K. Supramolecular Nanodevices: From Design Validation to Theranostic Nanomedicine. *Accounts Chem Res* **44**, 999-1008, doi:Doi 10.1021/Ar200094a (2011).

130 Lee, J. E., Lee, N., Kim, T., Kim, J. & Hyeon, T. Multifunctional Mesoporous Silica Nanocomposite Nanoparticles for Theranostic Applications. *Accounts Chem Res* **44**, 893-902, doi:Doi 10.1021/Ar2000259 (2011).

131 Ahrens, E. T., Flores, R., Xu, H. Y. & Morel, P. A. In vivo imaging platform for tracking immunotherapeutic cells. *Nat Biotechnol* **23**, 983-987, doi:Doi 10.1038/Nbt1121 (2005).

132 Du, W. *et al.* Amphiphilic hyperbranched fluoropolymers as nanoscopic 19F magnetic resonance imaging agent assemblies. *Biomacromolecules* **9**, 2826-2833, doi:10.1021/bm800595b (2008).

133 Du, W. J. *et al.* F-19- and Fluorescently Labeled Micelles as Nanoscopic Assemblies for Chemotherapeutic Delivery. *Bioconjugate Chem* **19**, 2492-2498, doi:Doi 10.1021/Bc800396h (2008).

134 Lammers, T., Hennink, W. E. & Storm, G. Tumour-targeted nanomedicines: principles and practice. *Brit J Cancer* **99**, 392-397, doi:Doi 10.1038/Sj.Bjc.6604483 (2008).

135 Whitehead, K. A., Langer, R. & Anderson, D. G. Knocking down barriers: advances in siRNA delivery. *Nat Rev Drug Discov* **8**, 129-138, doi:Doi 10.1038/Nrd2742 (2009).

136 Yang, X. Q., Grailer, J. J., Pilla, S., Steeber, D. A. & Gong, S. Q. Tumor-Targeting, pH-Responsive, and Stable Unimolecular Micelles as Drug Nanocarriers for Targeted Cancer Therapy. *Bioconjugate Chem* **21**, 496-504, doi:Doi 10.1021/Bc900422j (2010).

137 Gulyaev, A. E. *et al.* Significant transport of doxorubicin into the brain with polysorbate 80-coated nanoparticles. *Pharmaceut Res* **16**, 1564-1569, doi:Doi 10.1023/A:1018983904537 (1999).

138 Geldenhuys, W., Mbimba, T., Bui, T., Harrison, K. & Sutariya, V. Brain-targeted delivery of paclitaxel using glutathione-coated nanoparticles for brain cancers. *J Drug Target* **19**, 837-845, doi:Doi 10.3109/1061186x.2011.589435 (2011).

139 Iversen, T. G., Skotland, T. & Sandvig, K. Endocytosis and intracellular transport of nanoparticles: Present knowledge and need for future studies. *Nano Today* **6**, 176-185, doi:Doi 10.1016/J.Nantod.2011.02.003 (2011).

140 Bareford, L. A. & Swaan, P. W. Endocytic mechanisms for targeted drug delivery. *Adv Drug Deliver Rev* **59**, 748-758, doi:Doi 10.1016/J.Addr.2007.06.008 (2007).

141 Panyam, J., Zhou, W. Z., Prabha, S., Sahoo, S. K. & Labhasetwar, V. Rapid endo-lysosomal escape of poly(DL-lactide-co-glycolide) nanoparticles: implications for drug and gene delivery. *Faseb J* **16**, doi:Unsp 0892-6638/02/0016-1217, Doi 10.1096/Fj.02-0088com (2002).

142 Khalil, I. A., Kogure, K., Akita, H. & Harashima, H. Uptake pathways and subsequent intracellular trafficking in nonviral gene delivery. *Pharmacol Rev* **58**, 32-45, doi:Doi 10.1124/Pr.58.1.8 (2006).

143 Shen, H. *et al.* Enhanced and prolonged cross-presentation following endosomal escape of exogenous antigens encapsulated in biodegradable nanoparticles. *Immunology* **117**, 78-88, doi:Doi 10.1111/J.1365-2567.2005.02268.X (2006).

144 Varkouhi, A. K., Scholte, M., Storm, G. & Haisma, H. J. Endosomal escape pathways for delivery of biologicals. *J Control Release* **151**, 220-228, doi:Doi 10.1016/J.Jconrel.2010.11.004 (2011).

145 Paillard, A., Hindre, F., Vignes-Colombeix, C., Benoit, J. P. & Garcion, E. The importance of endo-lysosomal escape with lipid nanocapsules for drug subcellular bioavailability. *Biomaterials* **31**, 7542-7554, doi:Doi 10.1016/J.Biomaterials.2010.06.024 (2010).

146 Mura, S., Nicolas, J. & Couvreur, P. Stimuli-responsive nanocarriers for drug delivery. *Nat Mater* **12**, 991-1003, doi:Doi 10.1038/Nmat3776 (2013).

147 You, J. *et al.* Effective Photothermal Chemotherapy Using Doxorubicin-Loaded Gold Nanospheres That Target EphB4 Receptors in Tumors. *Cancer Res* **72**, 4777-4786, doi:Doi 10.1158/0008-5472.Can-12-1003 (2012).

148 Rapoport, N. Y., Kennedy, A. M., Shea, J. E., Scaife, C. L. & Nam, K. H. Controlled and targeted tumor chemotherapy by ultrasound-activated nanoemulsions/microbubbles. *J Control Release* **138**, 268-276, doi:Doi 10.1016/J.Jconrel.2009.05.026 (2009).

149 Qin, J. *et al.* Injectable Superparamagnetic Ferrogels for Controlled Release of Hydrophobic Drugs. *Adv Mater* **21**, 1354-1357, doi:Doi 10.1002/Adma.200800764 (2009).

150 Chen, K. J. *et al.* A Thermoresponsive Bubble-Generating Liposomal System for Triggering Localized Extracellular Drug Delivery. *Acs Nano* **7**, 438-446, doi:Doi 10.1021/Nn304474j (2013).

151 Zeng, X. H., Morgenstern, R. & Nystrom, A. M. Nanoparticle-directed sub-cellular localization of doxorubicin and the sensitization breast cancer cells by circumventing GST-Mediated drug resistance. *Biomaterials* **35**, 1227-1239, doi:Doi 10.1016/J.Biomaterials.2013.10.042 (2014).

152 Meng, H. A. *et al.* Engineered Design of Mesoporous Silica Nanoparticles to Deliver Doxorubicin and P-Glycoprotein siRNA to Overcome Drug Resistance in a Cancer Cell Line. *Acs Nano* **4**, 4539-4550, doi:Doi 10.1021/Nn100690m (2010).

153 Ke, H. T. *et al.* Gold-Nanoshelled Microcapsules: A Theranostic Agent for Ultrasound Contrast Imaging and Photothermal Therapy. *Angew Chem Int Edit* **50**, 3017-3021, doi:Doi 10.1002/Anie.201008286 (2011).

154 Lammers, T., Aime, S., Hennink, W. E., Storm, G. & Kiessling, F. Theranostic Nanomedicine. *Accounts Chem Res* **44**, 1029-1038, doi:Doi 10.1021/Ar200019c (2011).

155 Yu, M. K. *et al.* Drug-loaded superparamagnetic iron oxide nanoparticles for combined cancer imaging and therapy in vivo. *Angew Chem Int Edit* **47**, 5362-5365, doi:Doi 10.1002/Anie.200800857 (2008).

156 Lee, G. Y. *et al.* Theranostic Nanoparticles with Controlled Release of Gemcitabine for Targeted Therapy and MRI of Pancreatic Cancer. *Acs Nano* **7**, 2078-2089, doi:Doi 10.1021/Nn3043463 (2013).

157 Duncan, R. The dawning era of polymer therapeutics. *Nat Rev Drug Discov* **2**, 347-360, doi:10.1038/nrd1088 (2003).

158 Jikei, M. & Kakimoto, M. Hyperbranched polymers: a promising new class of materials. *Prog Polym Sci* **26**, 1233-1285, doi:Doi 10.1016/S0079-6700(01)00018-1 (2001).

159 Kesharwani, P., Jain, K. & Jain, N. K. Dendrimer as nanocarrier for drug delivery. *Prog Polym Sci* **39**, 268-307, doi:Doi 10.1016/J.Progpolymsci.2013.07.005 (2014).

160 Inoue, K. Functional dendrimers, hyperbranched and star polymers. *Prog Polym Sci* **25**, 453-571, doi:Doi 10.1016/S0079-6700(00)00011-3 (2000).

161 Gao, C. & Yan, D. Hyperbranched polymers: from synthesis to applications. *Prog Polym Sci* **29**, 183-275, doi:Doi 10.1016/J.Progpolymsci.2003.12.002 (2004).

162 Schull, C. & Frey, H. Controlled Synthesis of Linear Polymers with Highly Branched Side Chains by "Hypergrafting": Poly(4-hydroxy styrene)-graft-hyperbranched Polyglycerol. *Acs Macro Lett* **1**, 461-464, doi:Doi 10.1021/Mz200250s (2012).

163 Patil, M. L. *et al.* Internally Cationic Polyamidoamine PAMAM-OH Dendrimers for siRNA Delivery: Effect of the Degree of Quaternization and Cancer Targeting. *Biomacromolecules* **10**, 258-266, doi:Doi 10.1021/Bm8009973 (2009).

164 Reul, R., Nguyen, J. & Kissel, T. Amine-modified hyperbranched polyesters as non-toxic, biodegradable gene delivery systems. *Biomaterials* **30**, 5815-5824, doi:Doi 10.1016/J.Biomaterials.2009.06.057 (2009).

165 Zeng, X. H. *et al.* Hyperbranched Copolymer Micelles as Delivery Vehicles of Doxorubicin in Breast Cancer Cells. *J Polym Sci Pol Chem* **50**, 280-288, doi:Doi 10.1002/Pola.25027 (2012).

166 Wood, K. C., Little, S. R., Langer, R. & Hammond, P. T. A family of hierarchically self-assembling linear-dendritic hybrid polymers for highly efficient targeted gene delivery. *Angew Chem Int Edit* **44**, 6704-6708, doi:Doi 10.1002/Anie.200502152 (2005).

167 Stover, T. C., Kim, Y. S., Lowe, T. L. & Kester, M. Thermoresponsive and biodegradable linear-dendritic nanoparticles for targeted and sustained release of a pro-apoptotic drug. *Biomaterials* **29**, 359-369, doi:Doi 10.1016/J.Biomaterials.2007.09.037 (2008).

168 Wu, Z. H. *et al.* Linear-Dendritic Polymeric Amphiphiles as Carriers of Doxorubicin-In Vitro Evaluation of Biocompatibility and Drug Delivery. *J Polym Sci Pol Chem* **50**, 217-226, doi:Doi 10.1002/Pola.25008 (2012).

169 Naahidi, S. *et al.* Biocompatibility of engineered nanoparticles for drug delivery. *J Control Release* **166**, 182-194, doi:Doi 10.1016/J.Jconrel.2012.12.013 (2013).

170 Xiao, Y. L. *et al.* Multifunctional unimolecular micelles for cancer-targeted drug delivery and positron emission tomography imaging. *Biomaterials* **33**, 3071-3082, doi:Doi 10.1016/J.Biomaterials.2011.12.030 (2012).

171 Li, X. J. *et al.* Amphiphilic multiarm star block copolymer-based multifunctional unimolecular micelles for cancer targeted drug delivery and MR imaging. *Biomaterials* **32**, 6595-6605, doi:Doi 10.1016/J.Biomaterials.2011.05.049 (2011).

172 Sun, X. K. *et al.* An assessment of the effects of shell cross-linked nanoparticle size, core composition, and surface PEGylation on in vivo biodistribution. *Biomacromolecules* **6**, 2541-2554, doi:Doi 10.1021/Bm050260e (2005).

173 Thurmond, K. B., Kowalewski, T. & Wooley, K. L. Shell cross-linked knedels: A synthetic study of the factors affecting the dimensions and properties of amphiphilic core-shell nanospheres. *J Am Chem Soc* **119**, 6656-6665, doi:Doi 10.1021/Ja9710520 (1997).

174 Liu, H. J., Chen, Y., Zhu, D. D., Shen, Z. & Stiriba, S. E. Hyperbranched polyethylenimines as versatile precursors for the preparation of different type of unimolecular micelles. *React Funct Polym* **67**, 383-395, doi:Doi 10.1016/J.Reactfunctpolym.2007.01.009 (2007).

175 Ng, K. K., Lovell, J. F. & Zheng, G. Lipoprotein-Inspired Nanoparticles for Cancer Theranostics. *Accounts Chem Res* **44**, 1105-1113, doi:Doi 10.1021/Ar200017e (2011).

176 McConathy, W. J., Nair, M. P., Paranjape, S., Mooberry, L. & Lacko, A. G. Evaluation of synthetic/reconstituted high-density lipoproteins as delivery vehicles for paclitaxel. *Anti-cancer drugs* **19**, 183-188, doi:10.1097/CAD.0b013e3282f1da86 (2008).

177 Krieger, M. *et al.* Reconstituted low density lipoprotein: a vehicle for the delivery of hydrophobic fluorescent probes to cells. *Journal of supramolecular structure* **10**, 467-478, doi:10.1002/jss.400100409 (1979).

178 Bricarello, D. A., Smilowitz, J. T., Zivkovic, A. M., German, J. B. & Parikh, A. N. Reconstituted lipoprotein: a versatile class of biologically-inspired nanostructures. *Acs Nano* **5**, 42-57, doi:10.1021/nn103098m (2011).

179 Chen, J. *et al.* Ligand conjugated low-density lipoprotein nanoparticles for enhanced optical cancer imaging in vivo. *J Am Chem Soc* **129**, 5798-5799, doi:10.1021/ja069336k (2007).

180 Glickson, J. D. *et al.* Lipoprotein nanoplatform for targeted delivery of diagnostic and therapeutic agents. *Molecular imaging* **7**, 101-110 (2008).

181 Zheng, G., Chen, J., Li, H. & Glickson, J. D. Rerouting lipoprotein nanoparticles to selected alternate receptors for the targeted delivery of cancer diagnostic and therapeutic agents. *Proceedings of the National Academy of Sciences of the United States of America* **102**, 17757-17762, doi:10.1073/pnas.0508677102 (2005).

182 Duivenvoorden, R. *et al.* A statin-loaded reconstituted high-density lipoprotein nanoparticle inhibits atherosclerotic plaque inflammation. *Nature communications* **5**, 3065, doi:10.1038/ncomms4065 (2014).

183 Zhang, L. *et al.* Lapatinib-incorporated lipoprotein-like nanoparticles: preparation and a proposed breast cancer-targeting mechanism. *Acta pharmacologica Sinica* **35**, 846-852, doi:10.1038/aps.2014.26 (2014).

184 Longati, P. *et al.* 3D pancreatic carcinoma spheroids induce a matrix-rich, chemoresistant phenotype offering a better model for drug testing. *Bmc Cancer* **13**, doi:Artn 95, Doi 10.1186/1471-2407-13-95 (2013).

185 Gillies, E. R. & Frechet, J. M. J. pH-responsive copolymer assemblies for controlled release of doxorubicin. *Bioconjugate Chem* **16**, 361-368, doi:Doi 10.1021/Bc049851c (2005).

186 Hawker, C. J., Lee, R. & Frechet, J. M. J. One-Step Synthesis of Hyperbranched Dendritic Polyesters. *J Am Chem Soc* **113**, 4583-4588, doi:Doi 10.1021/Ja00012a030 (1991).

187 Wu, P. *et al.* Multivalent, bifunctional dendrimers prepared by click chemistry. *Chem Commun*, 5775-5777, doi:Doi 10.1039/B512021g (2005).

188 Padilla De Jesus, O. L., Ihre, H. R., Gagne, L., Frechet, J. M. & Szoka, F. C., Jr. Polyester dendritic systems for drug delivery applications: in vitro and in vivo evaluation. *Bioconjug Chem* **13**, 453-461 (2002).

189 Almutairi, A. *et al.* Biodegradable dendritic positron-emitting nanoprobes for the noninvasive imaging of angiogenesis. *Proceedings of the National Academy of Sciences of the United States of America* **106**, 685-690, doi:10.1073/pnas.0811757106 (2009).

190 Feliu, N. *et al.* Stability and biocompatibility of a library of polyester dendrimers in comparison to polyamidoamine dendrimers. *Biomaterials* **33**, 1970-1981, doi:Doi 10.1016/J.Biomaterials.2011.11.054 (2012).

191 Prabaharan, M., Grailer, J. J., Pilla, S., Steeber, D. A. & Gong, S. Amphiphilic multi-arm-block copolymer conjugated with doxorubicin via pH-sensitive hydrazone bond for tumor-targeted drug delivery. *Biomaterials* **30**, 5757-5766, doi:10.1016/j.biomaterials.2009.07.020 (2009).

192 Kwon, H. Y., Lee, J. Y., Choi, S. W., Jang, Y. S. & Kim, J. H. Preparation of PLGA nanoparticles containing estrogen by emulsification-diffusion method. *Colloid Surface A* **182**, 123-130, doi:Doi 10.1016/S0927-7757(00)00825-6 (2001).

193 Tewes, F. *et al.* Comparative study of doxorubicin-loaded poly(lactide-co-glycolide) nanoparticles prepared by single and double emulsion methods. *Eur J Pharm Biopharm* **66**, 488-492, doi:Doi 10.1016/J.Ejpb.2007.02.016 (2007).

194 Vetvicka, D. *et al.* Biological evaluation of polymeric micelles with covalently bound doxorubicin. *Bioconjug Chem* **20**, 2090-2097, doi:10.1021/bc900212k (2009).

195 Talelli, M. *et al.* Core-crosslinked polymeric micelles with controlled release of covalently entrapped doxorubicin. *Biomaterials* **31**, 7797-7804, doi:Doi 10.1016/J.Biomaterials.2010.07.005 (2010).

196 Schmaljohann, D. Thermo- and pH-responsive polymers in drug delivery. *Adv Drug Deliver Rev* **58**, 1655-1670, doi:Doi 10.1016/J.Addr.2006.09.020 (2006).

197 Hruby, M., Konak, C. & Ulbrich, K. Polymeric micellar pH-sensitive drug delivery system for doxorubicin. *J Control Release* **103**, 137-148, doi:Doi 10.1016/J.Jconrel.2004.11.017 (2005).

198 Du, J. Z., Du, X. J., Mao, C. Q. & Wang, J. Tailor-Made Dual pH-Sensitive Polymer-Doxorubicin Nanoparticles for Efficient Anticancer Drug Delivery. *J Am Chem Soc* **133**, 17560-17563, doi:Doi 10.1021/Ja207150n (2011).

199 Jin, Y. *et al.* Oxime Linkage: A Robust Tool for the Design of pH-Sensitive Polymeric Drug Carriers. *Biomacromolecules* **12**, 3460-3468, doi:Doi 10.1021/Bm200956u (2011).

200 Lundberg, P. *et al.* pH-triggered self-assembly of biocompatible histamine-functionalized triblock copolymers. *Soft Matter* **9**, 82-89, doi:Doi 10.1039/C2sm26996a (2013).

201 Park, J. *et al.* PEGylated PLGA nanoparticles for the improved delivery of doxorubicin. *Nanomedicine : nanotechnology, biology, and medicine* **5**, 410-418, doi:10.1016/j.nano.2009.02.002 (2009).

202 Kontoyianni, C. *et al.* A novel micellar PEGylated hyperbranched polyester as a prospective drug delivery system for paclitaxel. *Macromol Biosci* **8**, 871-881, doi:Doi 10.1002/Mabi.200800015 (2008).

203 Hucknall, A., Rangarajan, S. & Chilkoti, A. In Pursuit of Zero: Polymer Brushes that Resist the Adsorption of Proteins. *Adv Mater* **21**, 2441-2446, doi:Doi 10.1002/Adma.200900383 (2009).

204 Gao, W. P., Liu, W. G., Christensen, T., Zalutsky, M. R. & Chilkoti, A. In situ growth of a PEG-like polymer from the C terminus of an intein fusion protein improves pharmacokinetics and tumor accumulation. *Proceedings of the National Academy of Sciences of the United States of America* **107**, 16432-16437, doi:Doi 10.1073/Pnas.1006044107 (2010).

205 Lutz, J. F. & Hoth, A. Preparation of ideal PEG analogues with a tunable thermosensitivity by controlled radical copolymerization of 2-(2-methoxyethoxy)ethyl methacrylate and oligo(ethylene glycol) methacrylate. *Macromolecules* **39**, 893-896, doi:Doi 10.1021/Ma0517042 (2006).

206 Fréchet, J. M. J. & Tomalia, D. A. *Dendrimers and other dendritic polymers*. (Wiley, 2001).

207 Gitsov, I., Wooley, K. L., Hawker, C. J., Ivanova, P. T. & Frechet, J. M. J. Synthesis and Properties of Novel Linear Dendritic Block-Copolymers - Reactivity of Dendritic Macromolecules toward Linear-Polymers. *Macromolecules* **26**, 5621-5627, doi:Doi 10.1021/Ma00073a014 (1993).

208 Ma, X. P. *et al.* Facile Synthesis of Polyester Dendrimers as Drug Delivery Carriers. *Macromolecules* **46**, 37-42, doi:Doi 10.1021/Ma301849a (2013).

209 Allen, C., Maysinger, D. & Eisenberg, A. Nano-engineering block copolymer aggregates for drug delivery. *Colloid Surface B* **16**, 3-27, doi:Doi 10.1016/S0927-7765(99)00058-2 (1999).

210 Kabanov, A. V., Batrakova, E. V. & Alakhov, V. Y. Pluronic (R) block copolymers as novel polymer therapeutics for drug and gene delivery. *J Control Release* **82**, 189-212, doi:Pii S0168-3659(02)00009-3, Doi 10.1016/S0168-3659(02)00009-3 (2002).

211 D'Emanuele, A. & Attwood, D. Dendrimer-drug interactions. *Adv Drug Deliver Rev* **57**, 2147-2162, doi:Doi 10.1016/J.Addr.2005.09.012 (2005).

212 Zeng, F. W. & Zimmerman, S. C. Dendrimers in supramolecular chemistry: From molecular recognition to self-assembly. *Chem Rev* **97**, 1681-1712, doi:Doi 10.1021/Cr9603892 (1997).

213 Prabaharan, M., Grailer, J. J., Pilla, S., Steeber, D. A. & Gong, S. Folate-conjugated amphiphilic hyperbranched block copolymers based on Boltorn H40, poly(L-lactide) and poly(ethylene glycol) for tumor-targeted drug delivery. *Biomaterials* **30**, 3009-3019, doi:10.1016/j.biomaterials.2009.02.011 (2009).

214 Chen, S., Zhang, X. Z., Cheng, S. X., Zhuo, R. X. & Gu, Z. W. Functionalized Amphiphilic Hyperbranched Polymers for Targeted Drug Delivery. *Biomacromolecules* **9**, 2578-2585, doi:Doi 10.1021/Bm800371n (2008).

215 Cao, W. Q., Zhou, J., Mann, A., Wang, Y. & Zhu, L. Folate-Functionalized Unimolecular Micelles Based on a Degradable Amphiphilic Dendrimer-Like Star Polymer for Cancer Cell-Targeted Drug Delivery. *Biomacromolecules* **12**, 2697-2707, doi:Doi 10.1021/Bm200487h (2011).

216 Cheng, R., Meng, F. H., Deng, C., Klok, H. A. & Zhong, Z. Y. Dual and multi-stimuli responsive polymeric nanoparticles for programmed site-specific drug delivery. *Biomaterials* **34**, 3647-3657, doi:Doi 10.1016/J.Biomaterials.2013.01.084 (2013).

217 Liu, T., Qian, Y. F., Hu, X. L., Ge, Z. S. & Liu, S. Y. Mixed polymeric micelles as multifunctional scaffold for combined magnetic resonance imaging contrast enhancement and targeted chemotherapeutic drug delivery. *J Mater Chem* **22**, 5020-5030, doi:Doi 10.1039/C2jm15092a (2012).

218 Gillies, E. R. & Frechet, J. M. J. Dendrimers and dendritic polymers in drug delivery. *Drug Discov Today* **10**, 35-43, doi:Pii S1359-6446(04)03276-3, Doi 10.1016/S1359-6446(04)03276-3 (2005).

219 Conner, S. D. & Schmid, S. L. Regulated portals of entry into the cell. *Nature* **422**, 37-44, doi:Doi 10.1038/Nature01451 (2003).

220 Nam, H. Y. *et al.* Cellular uptake mechanism and intracellular fate of hydrophobically modified glycol chitosan nanoparticles. *J Control Release* **135**, 259-267, doi:10.1016/j.jconrel.2009.01.018 (2009).

221 Henry, S. M., El-Sayed, M. E., Pirie, C. M., Hoffman, A. S. & Stayton, P. S. pH-responsive poly(styrene-alt-maleic anhydride) alkylamide copolymers for intracellular drug delivery. *Biomacromolecules* **7**, 2407-2414, doi:10.1021/bm060143z (2006).

222 Torchilin, V. P. Recent approaches to intracellular delivery of drugs and DNA and organelle targeting. *Annu Rev Biomed Eng* **8**, 343-375, doi:Doi 10.1146/Annurev.Bioeng.8.061505.095735 (2006).

223 Guo, S. T. & Huang, L. Nanoparticles Escaping RES and Endosome: Challenges for siRNA Delivery for Cancer Therapy. *J Nanomater*, doi:Artn 742895, Doi 10.1155/2011/742895 (2011).

224 Sauer, A. M. *et al.* Role of endosomal escape for disulfide-based drug delivery from colloidal mesoporous silica evaluated by live-cell imaging. *Nano Lett* **10**, 3684-3691, doi:10.1021/nl102180s (2010).

225 Selbo, P. K. *et al.* Photochemical internalization provides time- and space-controlled endolysosomal escape of therapeutic molecules. *J Control Release* **148**, 2-12, doi:10.1016/j.jconrel.2010.06.008 (2010).

226 Tseng, C. L. *et al.* Development of gelatin nanoparticles with biotinylated EGF conjugation for lung cancer targeting. *Biomaterials* **28**, 3996-4005, doi:10.1016/j.biomaterials.2007.05.006 (2007).

227 Akinc, A., Thomas, M., Klibanov, A. M. & Langer, R. Exploring polyethylenimine-mediated DNA transfection and the proton sponge hypothesis. *J Gene Med* **7**, 657-663, doi:Doi 10.1002/Jgm.696 (2005).

228 Lechardeur, D., Verkman, A. S. & Lukacs, G. L. Intracellular routing of plasmid DNA during non-viral gene transfer. *Adv Drug Deliver Rev* **57**, 755-767, doi:Doi 10.1016/J.Addr.2004.12.008 (2005).

229 Yu, C. M. *et al.* Facile preparation of pH-sensitive micelles self-assembled from amphiphilic chondroitin sulfate-histamine conjugate for triggered intracellular drug release. *Colloid Surface B* **115**, 331-339, doi:Doi 10.1016/J.Colsurfb.2013.12.023 (2014).

230 Shrestha, R., Elsabahy, M., Florez-Malaver, S., Samarajeewa, S. & Wooley, K. L. Endosomal escape and siRNA delivery with cationic shell crosslinked knedel-like nano particles with tunable buffering capacities. *Biomaterials* **33**, 8557-8568, doi:Doi 10.1016/J.Biomaterials.2012.07.054 (2012).

231 Janib, S. M., Moses, A. S. & MacKay, J. A. Imaging and drug delivery using theranostic nanoparticles. *Adv Drug Deliver Rev* **62**, 1052-1063, doi:Doi 10.1016/J.Addr.2010.08.004 (2010).

232 Kelkar, S. S. & Reineke, T. M. Theranostics: Combining Imaging and Therapy. *Bioconjugate Chem* **22**, 1879-1903, doi:Doi 10.1021/Bc200151q (2011).

233 Patra, H. K. *et al.* MRI-Visual Order-Disorder Micellar Nanostructures for Smart Cancer Theranostics. *Adv Healthc Mater* **3**, 526-535, doi:Doi 10.1002/Adhm.201300225 (2014).

234 Chen, Y. *et al.* Manganese oxide-based multifunctionalized mesoporous silica nanoparticles for pH-responsive MRI, ultrasonography and circumvention of MDR in cancer cells. *Biomaterials* **33**, 7126-7137, doi:10.1016/j.biomaterials.2012.06.059 (2012).

235 Lee, J. E., Lee, N., Kim, T., Kim, J. & Hyeon, T. Multifunctional mesoporous silica nanocomposite nanoparticles for theranostic applications. *Acc Chem Res* **44**, 893-902, doi:10.1021/ar2000259 (2011).

236 Heo, D. N. *et al.* Gold nanoparticles surface-functionalized with paclitaxel drug and biotin receptor as theranostic agents for cancer therapy. *Biomaterials* **33**, 856-866, doi:Doi 10.1016/J.Biomaterials.2011.09.064 (2012).

237 Liu, Y. & Zhang, N. Gadolinium loaded nanoparticles in theranostic magnetic resonance imaging. *Biomaterials* **33**, 5363-5375, doi:10.1016/j.biomaterials.2012.03.084 (2012).

238 Xie, J., Lee, S. & Chen, X. Nanoparticle-based theranostic agents. *Adv Drug Deliv Rev* **62**, 1064-1079, doi:10.1016/j.addr.2010.07.009 (2010).

239 Gautier, J., Allard-Vannier, E., Munnier, E., Souce, M. & Chourpa, I. Recent advances in theranostic nanocarriers of doxorubicin based on iron oxide and gold nanoparticles. *J Control Release* **169**, 48-61, doi:Doi 10.1016/J.Jconrel.2013.03.018 (2013).

240 Atanasijevic, T., Shusteff, M., Fam, P. & Jasanoff, A. Calcium-sensitive MRI contrast agents based on superparamagnetic iron oxide nanoparticles and calmodulin. *Proceedings of the National Academy of Sciences of the United States of America* **103**, 14707-14712, doi:Doi 10.1073/Pnas.0606749103 (2006).

241 Pan, D., Lanza, G. M., Wickline, S. A. & Caruthers, S. D. Nanomedicine: perspective and promises with ligand-directed molecular imaging. *Eur J Radiol* **70**, 274-285, doi:10.1016/j.ejrad.2009.01.042 (2009).

242 Pandey, M. K. *et al.* Design and synthesis of perfluorinated amphiphilic copolymers: Smart nanomicelles for theranostic applications. *Polymer* **52**, 4727-4735, doi:Doi 10.1016/J.Polymer.2011.08.017 (2011).

243 Knight, J. C., Edwards, P. G. & Paisey, S. J. Fluorinated contrast agents for magnetic resonance imaging; a review of recent developments. *Rsc Adv* **1**, 1415-1425, doi:Doi 10.1039/C1ra00627d (2011).

244 Rolfe, B. E. *et al.* Multimodal Polymer Nanoparticles with Combined F-19 Magnetic Resonance and Optical Detection for Tunable, Targeted, Multimodal Imaging in Vivo. *J Am Chem Soc* **136**, 2413-2419, doi:Doi 10.1021/Ja410351h (2014).